日 中 笹 川 医 学 奨 学 金 制 度

第３６期研究者研究報告会

研 究 報 告 集

2014 年 5 月～2015 年 4 月

公益財団法人 日中医学協会

２０１５ 年 ４ 月 ３０ 日

日本財団ビル会議室１、２

目　次（発表順）

後発白内障に対する Nd:YAG レーザー後嚢切開術前後の光学特性，視機能および視覚関連 QOL の変化

研 究 者 氏 名 　　権　伍勇（第 36期笹川医学研究者）

中国所属機関 　　厦門長庚医院眼科

日本研究機関 　　筑波大学医学医療系眼科学

指 導 責 任 者 　　大鹿　哲郎　教授

共同研究者名 　　平岡孝浩　講師，山本敏哉　医師

　目　的：後発白内障に対し Neodymium:Yttrium-Aluminum-Garnet Laser（以下，YAG レーザー）後嚢切開術前後の光学特性，視機能および視覚に関連した生活の質 quality of life（以下，QOL）の変化について検討した．

　対象と方法：後発白内障と診断され YAG レーザー後嚢切開術を行った 16 例 20 眼（男性 7 名，女性 9 名，平均年齢 69.3 ± 6.8 歳）を対象とした．検討項目は，矯正視力，コントラスト感度，後方散乱，前方散乱，視覚関連 QOL で，術前と術後 1 週 術後 1 カ月で評価した 視覚関連 QOL は The 25-Item National Eye Institute Visual Function Questionnaire（以下，VFQ-25）を用いて評価した．

　結　果：矯正視力，コントラスト感度，後方散乱，前方散乱，VFQ-25 総合得点は術前と比べて術後 1 週と術後 1 カ月で統計学的有意差を認めた．術後 1 週と術後 1 カ月を比べても各パラメータで改善傾向を示したが，グレアありの条件下の薄暮視コントラスト感度以外は有意な差を認めなかった．VFQ-25 では，“色覚”を除いたすべての下位尺度に有意な改善が認められた．内容は “健康全般”，“視覚全般”，“遠見視力行動”，“心の健康”，“役割制限” および “運伝” が術前と術後 1 週，術後 1 カ月の間に，“眼痛”，“社会生活機能” は術前と術後 1 カ月，術後 1 週と術後 1 カ月の間に，“近見視力行動” については術前，術後 1 週，術後 1 カ月のそれぞれの間に，“自立” は術後 1 週と術後 1 カ月の間のみに有意な差を認めた．

　結　論：後発白内障に対し YAG レーザー後嚢切開術を行うことによって光学特性，視機能および視覚関連 QOL が改善することが定量的に示された．

　キーワード：後発白内障，YAG レーザー後嚢切開術，光学特性，視機能，視覚関連 QOL

［緒　言］

　後発白内障は白内障術後に最も多く生じる合併症であり，水晶体嚢内に残存した水晶体上皮細胞が増殖することで起こる後嚢混濁である[1]．後発白内障の治療は，観血的に後嚢を切開する手術から現在は非観血的な Neodymium:Yttrium-Aluminum-Garnet Laser（以下，YAG レーザー）後嚢切開術が標準的治療としての地位を確立している[2]．治療の決定時期は患者の視力低下やぼやけ，かすみなどの自覚症状に加え，細隙灯検査における後嚢混濁の所見が主体となって判断されている．また後発白内障を抑制するためのさまざまな研究が進んでいるが，現時点では完全に予防する方法はない．

　後発白内障が視機能に及ぼす影響の評価として，これまでに視力，コントラスト感度，立体視，散乱光などさまざまなパラメータが用いられてきた[3]．なかでも散乱光が視機能へ及ぼす影響が近年注目されている．過去の報告では，散乱光量測定は特に初期後発白内障に対しての治療適応や白内障手術術後予測を向上するための有効な指標になると考えられている[4]．しかし，後発白内障に対する YAG レーザー後嚢切開術後の

散乱光，特に前方散乱の変化に関してはまだ報告が少ない[5].

　今回，我々は治療時期の決定因子となり得る可能性のある散乱光に注目し，後発白内障眼における後方散乱と前方散乱を YAG レーザー後嚢切開術前後で比較した．また視力とコントラスト感度も同時に測定することによって散乱光が視機能へどのように影響しているのかを検討した．さらに，患者の視覚関連 QOL への影響も評価した．

[対象および方法]

1. 対象
　2014 年 6 月から 2015 年 2 月までの間に筑波大学附属病院眼科外来を受診した後発白内障患者のうちインフォームドコンセントが得られた症例を対象とした．
　散瞳後の瞳孔径が 6.5mm 以上得られなかった症例および治療を必要とした他の眼疾患（糖尿病黄斑浮腫など）の既往のある症例は除外した．

2. 方法
　すべての症例に対して，矯正視力，コントラスト感度，後方散乱，前方散乱，視覚関連 QOL 評価を YAG レーザー後嚢切開術の術前と術後 1 週，術後 1 カ月で測定した．

2.1 **YAG レーザー後嚢切開術**
　外来で後発白内障眼を散瞳後（ミドリン®P 点眼液，日本参天製薬），点眼麻酔下で YAG レーザー用のコンタクトレンズを装着させ，YAG レーザー（LUMENIS Inc, CA, U.S.A.）を用い通常 0.8〜1.0mJ 程度の低エネルギーから照射を開始した．切開が得られない場合にはエネルギーを上げていき，最終的に直径 5mm×5mm 程度の後嚢切開創を作製した．YAG レーザー後嚢切開術後一過性眼圧上昇の予防を目的として塩酸アプラクロニジン（アイオピジン®UD 点眼液，日本アルコン製薬）点眼液を術前後にそれぞれ 1 滴ずつ点眼した．

2.2 **視力**
　矯正視力は，オートレフケラトメーター（RC-5000, TOMEY Co., Nagoya, Japan）より得られた予測屈折値から屈折矯正を行い，明室（室内照度は視標輝度を上回らない）で 100%コントラストのランドルト環視標（VC-50, Takagi Seiko Co., Nagano, Japan）を用いて 5m の検眼距離で測定した．同じ段の視標が半数以上判読できる最小視標を求め，その視力値を矯正視力とした．

2.3 **コントラスト感度**
　コントラスト感度は，Optec-6500（Stereo Optical Co., Inc., IL, U.S.A.）を用いて完全矯正下で，薄暮視，グレアありの薄暮視，明所視，グレアありの明所視の 4 条件で測定した．また，コントラスト感度を定量化する一つの方法としてコントラスト感度曲線の下方の面積 area under the log contrast sensitivity function（以下，AULCSF）を算出し，統計解析に使用した．

2.4 **後方散乱**
　後方散乱は，散瞳後に前眼部画像撮影解析装置 EAS-1000（NIDEK Co, Ltd., Aichi, Japan）を用いて，0°, 45°, 90°および 135°の 4 方向でスリットを撮影し，散乱光強度として各方向の IOL 後面の光学部 3mm×0.25mm

エリアの平均濃度を算出した．さらに4方向の平均値を求め後方散乱の定量的指標とした．単位は本機が定めた単位 CCT（computer compatible tape）とした．

2.5 前方散乱

前方散乱は，C-Quant（OCULUS Inc., WA, U.S.A.）を用いて，眼内透光体の光散乱によって生じる網膜上への迷光の量，つまり眼内迷光値を測定した．C-Quant は中心ディスクを左右の2つの半円に分け，左右どちらの半円がよりフリッカーしているかを答えてもらう補正比較法に基づいた主観的な検査法である．眼内迷光値の結果は迷光補正レベル Log(s)として表示され，Log(s)値が高いほど，散乱が多いことを示す．

2.6 視覚関連 QOL 評価

視覚の質として日本語版 VFQ-25 のアンケート用紙を用いて自己記入式で調査を行った．VFQ-25 アンケートは 25 項目の質問から構成され，それぞれを"健康全般"，"視覚全般"，"眼痛"，"近見視力行動"，"遠見視力行動"，"社会生活機能"，"心の健康"，"役割制限"，"自立"，"運転"，"色覚"，"周辺視野"の 12 の下位尺度に分類し，これらの下位尺度を 0〜100 点に変換して評価する．点数が良いほど患者の視覚関連 QOL が高いことを示す．12 の下位尺度のうち，"健康全般"を除く 11 の下位尺度の平均を総合得点として算出し，視覚関連 QOL 全体の評価として用いた．

2.7 統計学分析

統計処理は StatView 5.0 ソフトウェア（SAS Institute Inc., NC, U.S.A.）を用い，治療前後の各期間の比較には repeated-measures analysis of variance（ANOVA）を施行し，有意差が認められた場合はさらに Fisher の PLSP test を用い多重比較検定を行った．$p < 0.05$ を統計学的有意差ありと判定した．すべてのデータは平均 ± 標準偏差で表示した．

［結 果］

対象者の内訳を表 1 に示す．男性 7 名，女性 9 名，年齢は 55〜81 歳（69.3 ± 6.8 歳）であった．白内障手術から YAG レーザー後嚢切開術施行までの期間は 11.8〜66 カ月（35.8 ± 13.2 カ月）であった．本研究の症例のなかで，4 例は両眼ともに後発白内障で 1 週の間隔をおいて左右眼別々に YAG レーザー治療を施行した．YAG レーザー治療後，すべての症例において軽度の飛蚊症以外に重篤な合併症はみられず経過良好であった．

表 1. 対象者の内訳

性別（男/女）	7/9
年齢（歳）	55〜81 歳（69.3 ± 6.8 歳）
眼別（片/両）	12/4
期間（月）	11.8〜66 カ月（35.8 ± 13.2 カ月）

YAG レーザー治療前後の各パラメータの変化を表 2 に示す．すべてのパラメータにおいて術前と比べて術後 1 週と術後 1 カ月で統計学的有意差を認めた．術後 1 週と比較して術後 1 カ月ではさらに改善傾向を示したが，グレアありの薄暮視 AULCSF 以外に統計学的有意差は認めなかった．

表 2. YAG レーザー治療前後の各パラメータの変化

パラーメータ	治療前	1 週	1 カ月	ANOVA P value	Fisher test P < 0.05
矯正視力（LogMAR）	0.34 ± 0.23	0.01 ± 0.11	0.00 ± 0.14	＜0.0001*	†¶
薄暮視 AULCSF	0.35 ± 0.37	1.30 ± 0.23	1.32 ± 0.33	＜0.0001*	†¶
薄暮視 AULCSF グレアあり	0.07 ± 0.19	0.88 ± 0.38	1.06 ± 0.37	＜0.0001*	†¶‡
明所視 AULCSF	0.52 ± 0.47	1.52 ± 0.28	1.56 ± 0.38	＜0.0001*	†¶
明所視 AULCSF グレアあり	0.37 ± 0.51	1.56 ± 0.31	1.61 ± 0.32	＜0.0001*	†¶
後方散乱（CCT）	52.29 ± 25.51	13.69 ± 12.99	13.59 ± 12.96	＜0.0001*	†¶
前方散乱（Log(s)）	1.54 ± 0.25	1.36 ± 0.31	1.27 ± 0.25	0.0064*	†¶
VFQ-25 総合得点	67.49 ± 12.76	81.52 ± 10.91	85.87 ± 9.73	＜0.0001*	†¶

LogMAR = logarithm of the minimum angle of resolution; AULCSF = area under the log contrast sensitivity function;

CCT = computer-compatible tape; Log(s) = log (stray light); VFQ-25 = The 25-item National Eye Institute visual function

questionnaire; ANOVA = analysis of variance

＊ 経時変化に統計学的有意差あり

† 術前と術後 1 週の間に統計学的有意差あり

¶ 術前と術後 1 カ月の間に統計学的有意差あり

‡ 術後 1 週と 1 カ月の間に統計学的有意差あり

　YAG レーザー治療前後の VFQ-25 における下位尺度の変化を表 3 に示す．"色覚"を除いたすべての下位尺度において有意な改善が認められ，"健康全般"，"視覚全般"，"遠見視力行動"，"心の健康"，"役割制限"および"運伝"は術前と術後 1 週，術後 1 カ月の間に，また"眼痛"，"社会生活機能"は術前と術後 1 カ月，術後 1 週と術後 1 カ月に，"近見視力行動"については術前，術後 1 週，1 カ月のそれぞれの間に，"自立"は術後 1 週と術後 1 カ月の間のみに統計学的有意差を認めた．

表 3. YAG レーザー治療前後の VFQ-25 下位尺度の変化

下位尺度	治療前	1 週	1 カ月	ANOVA P value	Fisher test P < 0.05
健康全般	40.00 ± 14.96	48.75 ± 15.12	52.50 ± 16.02	0.0002*	†¶
視覚全般	52.00 ± 18.81	80.00 ± 11.24	80.00 ± 11.24	＜0.0001*	†¶
眼痛	77.50 ± 21.31	80.63 ± 18.79	88.13 ± 11.81	0.0038*	¶‡
近見視力行動	51.67 ± 19.04	72.50 ± 15.32	81.67 ± 13.41	＜0.0001*	†¶‡
遠見視力行動	62.50 ± 13.11	82.08 ± 10.22	84.17 ± 9.33	＜0.0001*	†¶
社会生活機能	80.63 ± 08.58	84.38 ± 10.63	91.25 ± 10.02	0.0003*	¶‡
心の健康	65.63 ± 20.23	80.63 ± 18.01	86.25 ± 14.85	＜0.0001*	†¶
役割制限	69.38 ± 21.64	85.63 ± 11.67	87.50 ± 13.45	＜0.0001*	†¶
自立	81.67 ± 20.52	87.92 ± 19.02	91.67 ± 14.31	0.0119*	¶
運転	61.81 ± 18.43	75.00 ± 21.86	79.86 ± 21.50	＜0.0001*	†¶
色覚	90.00 ± 12.57	95.00 ± 10.26	93.75 ± 11.11	0.1132	
周辺視野	58.75 ± 16.77	73.75 ± 18.98	81.25 ± 21.27	＜0.0001*	†¶

VFQ-25 = The 25-item National Eye Institute visual function questionnaire; ANOVA = analysis of variance

＊ 経時変化に統計学的有意差あり

† 術前と術後 1 週の間に統計学的有意差あり

¶ 術前と術後 1 カ月の間に統計学的有意差あり

‡ 術後 1 週と術後 1 カ月の間に統計学的有意差あり

［考　按］

　　後発白内障の主な自覚症状として，視力低下，霧視，グレアなどが挙げられる．YAG レーザー後嚢切開術治療を受ける患者にとって最も関心の高い点は，これらの自覚症状の改善である．今回我々の検討では，術後 1 週の時点で矯正視力の有意な改善が認められた．これは過去の報告とも一致している[6]．また，コントラスト感度においても術後 1 週から有意な改善を示し術後 1 カ月までさらに改善する傾向を示した．特にグレアありの薄暮視コントラスト感度が術前には著しく障害されていたが，術後 1 週には大きく改善し，術後 1 カ月でもさらなる改善を示した．薄暮視かつグレアありの条件は最も過酷な条件であるため，この条件下のコントラスト感度が最も鋭敏に変化したと考えられる．コントラスト感度は，視覚の質 quality of vision（QOV）を評価できる検査であり[7]，また，日常生活における適応，移動，読書，運転などに必要とする視機能と非常にいい相関があることが知られている[8]．コントラスト感度測定は，術前視力が良好でも霧視などの自覚症状があれば積極的に行うことによって後発白内障の治療時期決定の参考になると考えられる．

　　また，後発白内障の YAG レーザー後嚢切開術治療評価として実用視力，収差，散乱など多方面から検討されている[9]．我々は光学特性の一つとして散乱の検討を行い，前方，後方散乱のいずれも術後 1 週から有意に改善することを見出した．これらのことより治療評価として後方散乱や前方散乱が指標となり得るであろう．一方，前方散乱の評価法として客観的に測定する Optical Quality Analysis System（以下，OQAS）と主観的に測定する C-Quant がある．OQAS はダブルパス技術に基づいて前方散乱を評価しているのに対し，C-Quant は補正比較法を利用して散乱光である眼内迷光値を測定し前方散乱を評価している．今回，先行研究より OQAS では術前前方散乱を測定できなかった症例が多数存在したため本研究の検討項目から除外した．これは後発白内障の後嚢混濁度の程度が機械の測定範囲を超えたからと考えられる．一方，C-Quant は術前の前方散乱評価が可能で，術前眼内迷光値 1.54 ± 0.25log(s)から術後 1 カ月で 1.27 ± 0.25log(s)へと有意な改善が認められた．同年代の眼内迷光値は 1.20log(s)であるため，正常値近くまで回復したことが理解できる．このことから後発白内障における治療評価として C-Quan は有用であると考えられる．過去の報告では，眼内迷光値測定は視力とは関連がなく白内障手術術後予測を向上するに有効な指標とも言われ，後発白内障に対しても同様に有効な指標になり得る可能性を考えている．

　　最後に，VFQ-25 は視覚に関連した健康関連 QOL を測定する尺度であり，今回，この方法を用いて YAG レーザー後嚢切開術前後の視覚関連 QOL を検討した．今回の検討では，VFQ-25 総合得点が術後 1 週から有意かつ大幅に改善し術後 1 カ月まで維持された．VFQ-25 は，生活場面における視機能と，見え方による身体的，心理的，社会的な生活側面の制限の程度を測定する下位尺度から構成されている．一方，色覚は術前後で変化がなかった．このことから，後発白内障は色覚に影響を及ぼさないということが考えられる．また大鹿らは，同じ日本語版 VFQ-25 を用いて検討した結果，白内障罹患によって患者の視覚関連 QOL は著しく障害されているが，白内障手術を行うことにより有意かつ大幅に改善することを報告し VFQ-25 の有用性を証明した．今回の検討から後発白内障において視覚関連 QOL 評価は治療効果の有用性を評価するのに非常に有用な検査と考えることができる．

数名の術者によって YAG レーザー治療が行われた点と切開された後嚢の形が統一されなかった点が本研究の限界として挙げられる．しかし，切開された後嚢の直径が 5mm 以上保たれば普通の生活には影響を与えないと指摘されており[10]，今回の症例においてはすべて 5mm 以上の切開が行われた．また，今回の後発白内障の評価については自覚的な検査が多かったことも問題点として挙げられるが，前眼部画像撮影解析装置 EAS-1000 のように客観性が高い評価方法による更なる検討が必要と考えられる．

　結論として，後発白内障に対して YAG レーザー後嚢切開術前後の光学特性，視機能および視覚関連 QOL を検討した結果，検討項目のすべてのパラメータ（視力，コントラスト感度，後方散乱，前方散乱，VFQ-25）が術後 1 週から有意な改善が認められるとともに術後 1 カ月まで保たれていることが示された．高齢化が深刻な問題となった現代社会で，視覚関連 QOL の改善は高齢者自身の生活だけでなく高齢化社会で起きた種々の問題の解決策の一つになり得るものと考えられる．

［文　献］

1.　McDonnell PJ, Zarbin MA, Green WR : Posterior capsule opacification in pseudophakic eyes. Ophthalmology. 1983;90:1548-1553.

2.　Aron-Rosa D : Use of a pulsed neodymium-Yag laser for anterior capsulotomy before extracapsular cataract extraction. J Am Intraocul Implant Soc. 1981;7:332-333.

3.　Magno BV, Datiles MB, Lasa MS, Fajardo MR, Caruso RC, Kaiser-Kupfer MI : Evaluation of visual function following neodymium:YAG laser posterior capsulotomy. Ophthalmology. 1997;104:1287-1293.

4.　van Bree MC, van den Berg TJ, Zijlmans BL : Posterior capsule opacification severity, assessed with straylight measurement, as main indicator of early visual function deterioration. Ophthalmology. 2013;120:20-33.

5.　van Bree MC, Zijlmans BL, van den Berg TJ : Effect of neodymium:YAG laser capsulotomy on retinal straylight values in patients with posterior capsule opacification. J Cataract Refract Surg. 2008;34:1681-1686.

6.　Oztas Z, Palamar M, Afrashi F, Yagci A : The effects of Nd:YAG laser capsulotomy on anterior segment parameters in patients with posterior capsular opacification. Clin Exp Optom. 2015;98:168-171.

7.　Cheng CY, Yen MY, Chen SJ, Kao SC, Hsu WM, Liu JH : Visual acuity and contrast sensitivity in different types of posterior capsule opacification. J Cataract Refract Surg. 2001;27:1055-1060.

8.　Leat SJ, Woodhouse JM : Reading performance with low vision aids: relationship with contrast sensitivity. Ophthalmic Physiol Opt. 1993;13:9-16.

9.　Wakamatsu TH, Yamaguchi T, Negishi K, Kaido M, Matsumoto Y, Ishida R, Kojima T, Ibrahim OM, Saiki M, Dogru M, Tsubota K : Functional visual acuity after neodymium:YAG laser capsulotomy in patients with posterior capsule opacification and good visual acuity preoperatively. J Cataract Refract Surg. 2011;37:258-264.

10.　Aslam TM, Dhillon B : Neodymium:YAG laser capsulotomy: a clinical morphological analysis. Graefes Arch Clin Exp Ophthalmol. 2002;240:972-976.

作成日：2015 年 4 月 10 日

Development of HPLC determination and transdermal penetration
of three Vitamin C derivatives
三種類のビタミンＣ誘導体の高速液体クロマトグラフィーの
定量条件の確立及び経皮吸収性の検討

研 究 者 氏 名　　　蔡　璐璐（第 36 期笹川医学研究者）
中国所属機関　　　電子科技大学臨床医学院四川省人民医院薬学部
日本研究機関　　　京都薬科大学薬剤学
指 導 責 任 者　　　山本　昌　教授
共同研究者名　　　サングアンガン和子

Abstract:

Vitamin C has many functions as a cosmetic ingredient including skin lightening promoting collagen synthesis and inhibiting lipid peroxidation. However, because of its poor penetration of the skin and its instability in formulations, many kinds of derivatives have been synthesized to overcome the short-coming of vitamin C. In this present study, three rapid HPLC methods were developed for the assay of the different vitamin C derivatives, including 3-o-cetyl ascorbic acid, ascorbyl dipalmitate and ascorbyl tetraisopalmitate. In addition, the solubilizer, polyoxyethylene 40 stearate, increased the solubility of the three derivatives, but did not interfere with their HPLC analysis. *In vitro* skin permeation study showed that among the formulations of vitamin C and its derivatives with or without solubilizer, ascorbyl tetraisopalmitate exhibited best percutaneous absorption, suggesting its potential use as a substitute of vitamin C in skin care and dermopathic therapy.

Keywords:

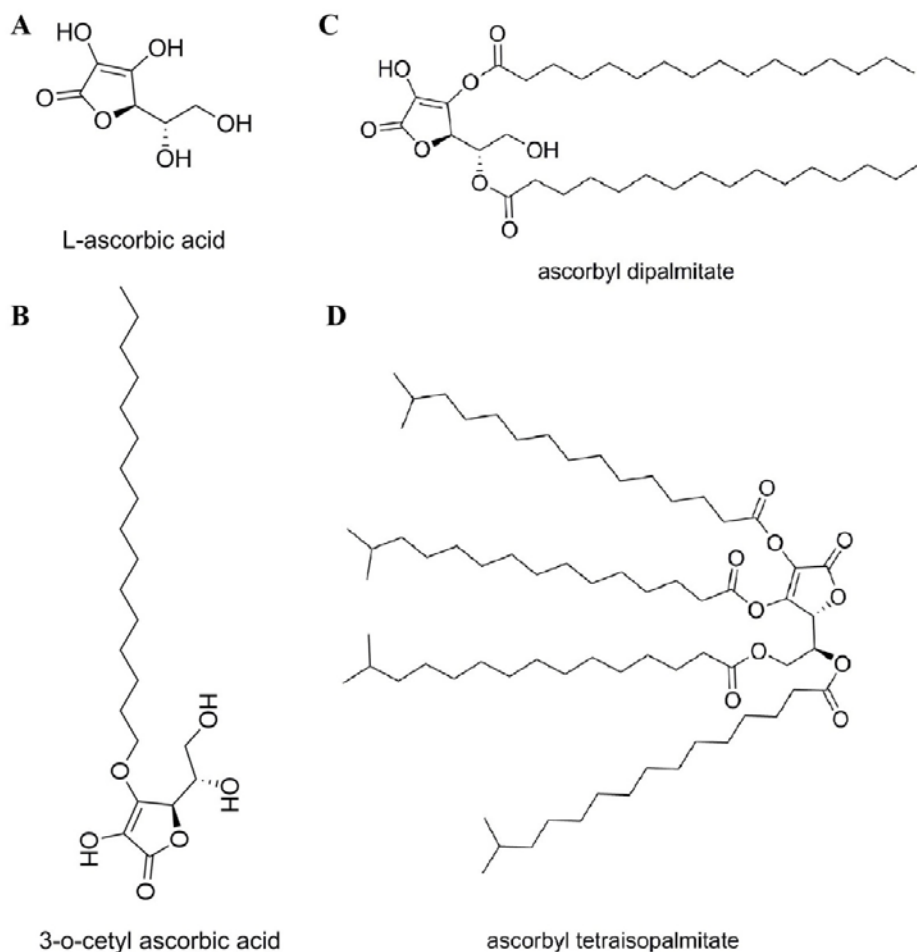Vitamin C derivative, HPLC determination, transdermal permeation, skin content

1. Introduction

The use of L-ascorbic acid (vitamin C) for topical application is not a new procedure. It has been used in pharmaceutical and cosmetic preparations for a long time on the basis of its many favorable effects on the skin [1]. However, free vitamin C is unstable, being easily oxidized and inactivated when exposed to air, and it also cannot penetrate across the skin because of its hydrophilicity [2].

Some marketed products containing unstable free vitamin forms need great investments in specific methods of packaging and containers and have short shelf-lives. Therefore, more stable and safer new delivery systems, such as microemulsions, microcapsules, nanospheres, liposomes [3] as well as the use of ester derivatives such as magnesium ascorbyl phosphate (PMG) and sodium ascorbyl phosphate (water-soluble derivatives) and ascorbyl-6-palmitate and tetra-isopalmitoyl ascorbic acid (IP) (liposoluble derivatives) are attempted to prolong formulation stability and are increasingly substituting the use of vitamin C free form [4, 5]. Moreover, liposoluble derivatives such as IP are able to better penetrate the skin [1] and have increased stability when compared to vitamin C free form [6].

3-O-Cetyl ascorbic acid (Cetyl), an oil-soluble vitamin C derivative, can improve quality and structural properties of collagen in skin, help to organize collagen fibers in perfect bundles, and boost collagen type I synthesis [7]. Ascorbyl dipalmitate (CP), oil soluble vitamin C derivative with anti-aging effect, ability of boosting HSP47 expression in skin and promoting collagen synthesis [8], is also a more stable form of ascorbic acid and has been used successfully in several formulations [9-10]. Tetra-isopalmitoyl ascorbic acid (IP), an oil-soluble vitamin C derivative with improved percutaneous absorption and stability, and ability of preventing lipid peroxidation, promoting collagen synthesis [11], is the first lipoidic-liquiform vitamin C derivative by itself in cosmetic formulations. Ochiai et al. [12] demonstrated 84% liberation of vitamin C by the derivative in reconstructed skin. IP, which has already been widely used as an additive in

cosmetic formulations, has also been approved as "quasi drugs" by Japanese authorities. Using these vitamin C derivatives seems promising in skin care and dermopathic therapy, as a result, it`s essential to quantitatively analyze these derivatives and evaluate their skin penetration ability. However, no method has been reported in literature for the quantitative analysis and skin penetration of Cetyl. In addition, few studies have been examined on the determination of IP and CP [9-10, 13].

A L-ascorbic acid

C ascorbyl dipalmitate

B 3-o-cetyl ascorbic acid

D ascorbyl tetraisopalmitate

Scheme 1 The structures of vitamin C (A), Cetyl (B), CP (C) and IP (D)

Table 1 The information of vitamin C and its derivatives.

Abbreviation	Full name	Formula	Molecular weight	Property
Vc	Ascorbic Acid / Vitamin C	$C_6H_8O_6$	176.12	hydrophilic
Cetyl	3-O-Cetyl Ascorbic Acid	$C_{22}H_{40}O_6$	400.55	lipophilic
CP	Ascorbyl Dipalmitate	$C_{38}H_{68}O_8$	652.95	lipophilic
IP	Ascorbyl Tetraisopalmitate	$C_{70}H_{128}O_{10}$	1229.76	lipophilic

Because all of Cetyl, IP and CP are hydrophobic with poor aqueous solubility, therefore, it`s necessary to develop feasible formulations for them to compare their skin penetration with vitamin C. Polyoxyethylene 40 stearate (Myrj 52), as the nonionic surfactant with a HLB value of 16.9, is freely soluble in water. It was used as a carrier to improve the dissolution of hydrophobic agents, such as cyclosporin A, griseofulvin, tolbutamide and indomethacin [14]. It was used as well as in some transdermal drug delivery system [15], such as emulsified gel and nanoliposome, to increase the solubility, promote emulsification and control stability during a shelf life of hydrophobic and unstable agents [16-17].

Based on the previous findings, the present study was aimed to develop the simple, reproducible and selective

HPLC methods for three different vitamin C derivatives, Cetyl, IP as well as CP. The aqueous formulations of these compounds were prepared with or without Myrj 52, and evaluated their penetration ability across the rat abdominal skin compared with vitamin C.

2. Materials and methods

2.1. Reagents

L (+)-ascorbic acid was obtained from Wako Pure Chemical Industries (Osaka, Japan). 3-O-CETYL, VC-CP and VC-IP were obtained from Nikkol Chemicals Co., Ltd. (Tokyo, Japan). Isopropanol, acetonitrile and methanol were HPLC grade, and obtained from Wako Pure Chemical Industries, Ltd. (Osaka, Japan). Myrj 52 was obtained from Sigma-Aldrich Co., Ltd. (St. Louis, MO, USA). All other chemicals were of analytical grade.

2.2. High-performance liquid chromatography (HPLC) method study

The HPLC method was performed using an equipment (Shimadzu® Corporation, Japan) consisted of a solvent delivery system, an auto injector fitted with a 20 µL loop, an online degasification system, a column thermostat oven and an UV/VIS photodiode array detector. The output signal was monitored and integrated using HPLC CBM-20A software (Shimadzu ® Co. Ltd., Japan). Separations were carried out on a HILIC column (4.6 × 150 mm I.D.; COSMOSIL®, Japan) or a 5C18-AR-2 column (4.6 × 150 mm I.D.; COSMOSIL®, Japan) and isocratically eluted with corresponding mobile phase. The mobile phase was prepared fresh each day and vacuum-filtered through a 0.45 µm pore filtration membrane (Millex ® HV: Millipore, Milford, CT, U.S.A.).Standard solutions were prepared in corresponding mobile phase, and stored in the dark at 4°C. Calibration curves were performed in the range of 10-500 µg/ml.

2.3. In vitro permeation studies

For *in vitro* skin permeation studies, Franz diffusion cell method was used. Vitamin C, Cetyl, CP and IP were prepared in the phosphate buffer saline (PBS, pH 7.4) with or without Myrj 52, and adjusted to pH 5 to yield a final concentration of 10 mg/ml. The concentration of Myrj 52 in the donor solution was 0, 2, and 10% (w/v) to study the effects of solubilizer.

Male Wistar rats (8 weeks old, 250g) were anesthetized with an intraperitoneal injection of sodium pentobarbital (40 mg/kg). The hair of the abdominal skin was carefully shaved, and then rats were sacrificed using procedures approved by the Experimental Animal Ethics Committee of Kyoto Pharmaceutical University. Thereafter, skin specimens were freshly excised from the abdominal region of the rats. After the subcutaneous fat was removed, the skin was cleaned with normal saline (NS) and frozen and stored at -20°C until use. The required pieces of skin were thawed at room temperature for 30 min before the skin permeation experiment.

For permeation studies, a piece of excised rat skin was mounted on a Franz-type diffusion cell with the stratum corneum facing the donor compartment. The donor compartment (0.5 ml) contained 10mg/ml Vitamin C, Cetyl, CP or IP in PBS with or without Myrj 52. The receptor compartment was filled with the same buffers as the donor but without vitamin C, Cetyl, CP or IP. The available diffusion area of the cell was 0.95 cm^2. The receptor compartment was maintained at 32 °C using a thermally controlled circulating water bath, and the contents were stirred with a magnetic bar. The length of the sampling period was 24h.

After the permeation studies, skin was cut to small pieces and homogenized. In addition, Cetyl was extracted by methanol, and CP was extracted by ethanol. The mixture was centrifuged at 7,000 rpm for 30 min. Then 250 µl of the supernatant was mixed with 250 µl of mobile phase. The solution was vortexed for 10 s and centrifuged at 12,000 rpm for 5 min. Finally, 10 µl clear supernatant of each sample was analyzed by HPLC. For IP, after homogenizing and centrifuging at 7,000 rpm for 30 min, 1ml of the permeation sample was mixed with 1ml ethanol, and evaporated at 70°C to remove the aqueous solvent. After redissolving by 1ml HPLC mobile phase, the resulting organic solution was centrifuged at 12,000 rpm for 5 min. Thereafter, 10 µl clear supernatant of each sample was analyzed by HPLC.

2.4. Statistical analyses

Results are expressed as the mean ± S.D. of at least three experiments. Statistical significances between groups were analyzed using Dunnet's test and T-test; $p < 0.05$ was considered to be significant.

3. Results

3.1. HPLC method study

As shown in Table 2 and Figure 1, the simple, reproducible and selective HPLC methods for Vc derivatives were established. For Vc, chromatographic separation was performed using a HILIC column (4.6 × 150 mm I.D.; COSMOSIL®, Japan) at 30°C. The mobile phase was acetonitrile / 0.1M ammonium acetate (60/40, v/v) at a flow rate of 1.0 ml/min. The wavelength of the UV detector was set at 265 nm. The retention time was approximately 11 min, and the calibration curve range was from 10 to 500 µg/ml for Vc (R^2= 0.9999). For Cetyl, CP and IP, chromatographic separation was performed using a 5C18-AR-2 column (150 ×4.6mm, COSMOSIL®, Japan) with UV detection at 246 nm, 240 nm and 222 nm, respectively. As mobile phase, methanol and ultrapure water (85/15, v/v), methanol and 0.1% TFA (98/2, v/v), and methanol and isopropanol (40/60, v/v) were used, respectively. The retention times were approximately 13.5 min, 8.5 min and 5.7 min, respectively. The calibration curve range was from 10 to 500 µg/ml, respectively, and R^2 ranged from 0.999 to 1.
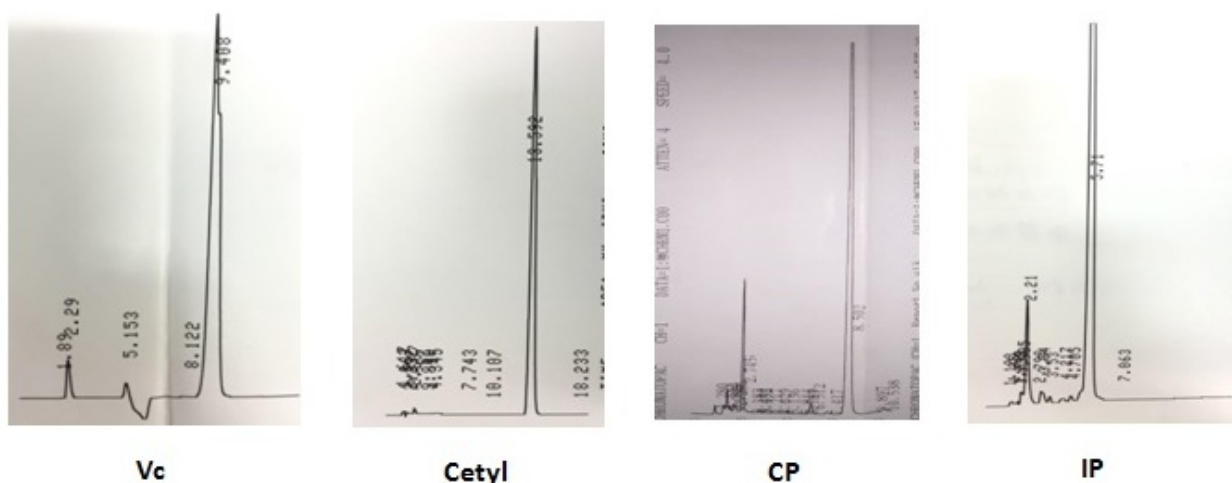

Figure 1 the HPLC spectra of Vc and its derivatives

Table 2 HPLC conditions of Vc and its derivatives

Compounds	Column	Mobile phase (V/V)	Flow rate (ml/min)	λ (nm)	RT (min)
Vc	HILIC (150 ×4.6mm)	Acetonitrile : Ammonium Acetate (0.1 M) = 80 : 20	1	254	9.4
Cetyl	5C18-AR-2 (150 ×4.6mm)	Methanol : KH$_2$PO$_4$ (0.05 M, pH = 3.5) = 85 : 15	1	246	13.5
IP	5C18-AR-2 (150 ×4.6mm)	Methanol : Isopropanol = 40 : 60	1	222	5.7
CP	5C18-AR-2 (150 ×4.6mm)	Methanol : TFA (0.1%, pH = 2.3) = 98 : 2	1	240	8.5

3.2. In vitro permeation studies

The amounts of Vc and its derivatives remaining in the skin were analyzed after the permeation studies. Figure 3 showed the skin content of Vc and its derivatives by percentage of the initial concentration in the donor. We found the skin content of IP without Myrj 52 was highest (10.5 ± 0.48%), followed by Cetyl with 2% Myrj 52 (7.43 ± 0.13%), IP

with 10% Myrj 52 (5.78 ± 0.79%), and IP with 2% Myrj 52 (5.53 ± 0.99%), respectively, which significantly increased the skin content as compared with Vc (0.82 ± 0.14%). They increased the skin retention by12.96, 8.15, 7.90 and 6.74-fold, respectively, as compared with Vc without Myrj 52.
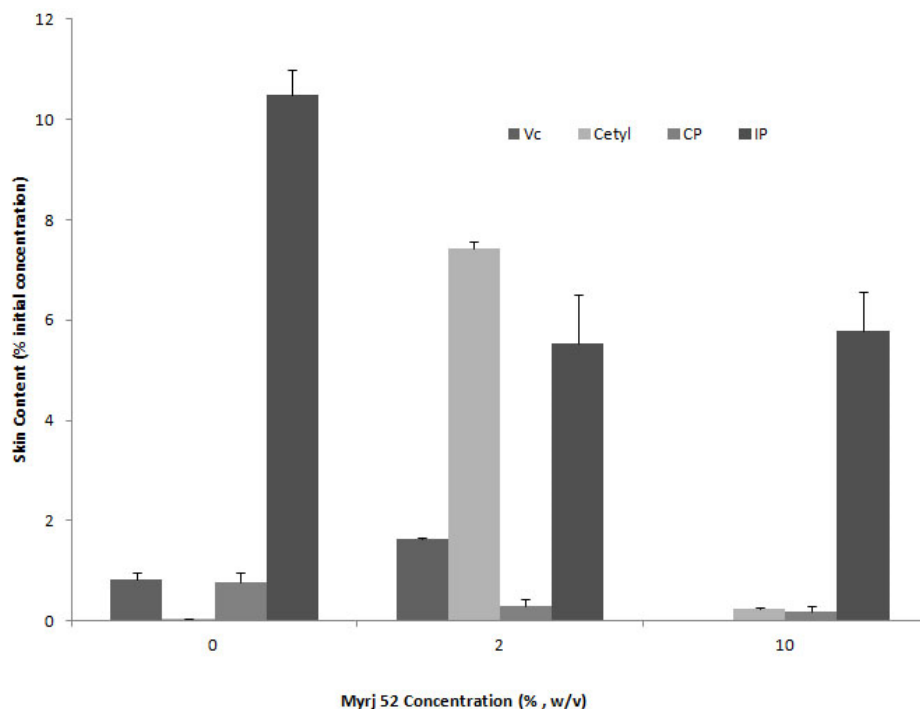
Figure 2 Skin content of Vc and its derivatives with or without 2-10% Myrj 52.

Note: Results are expressed as the mean ± S.D. of at least 3 experiments. *$p < 0.05$ were considered to be statistically significant compared with the Vc without Myrj 52 group.

4. Discussion

In the present study, we developed three rapid HPLC methods for the determination of 3 different vitamin C derivatives and the methods presented good linearity and selectivity. Because of the different structures and properties among Cetyl, CP and IP, their determination methods were different in mobile phase, pH, wavelength and retention time. In addition, the solubilizer, Myrj 52, had no UV absorption from 210 to 270 nm; therefore, it did not interfere with the HPLC analysis of vitamin C derivatives.

Even though, our results showed the Cetyl and IP penetrated the skin more than Vc *in vitro*, suggesting their potential use as the substitutes of vitamin C in skin care and dermopathic therapy, however, the rate of their conversion to Vc and *in vivo* skin penetration ability need further study.

References and Notes:

1. Gosenca, Mirjam, et al. A new approach for increasing ascorbyl palmitate stability by addition of non-irritant co-antioxidant. *AAPS PharmSciTech*, 11, 1485-14923 (2010).

2. Hsiao, Chien-Yu, et al. Skin pretreatment with lasers promotes the transdermal delivery of vitamin C derivatives. *Lasers in Medical Science*, 26, 369-376 (2011).

3. Kaur, Indu P., Meenakshi Kapila, et al. Role of novel delivery systems in developing topical antioxidants as therapeutics to combat photoageing. *Ageing Research Reviews*, 6, 271-288 (2007).

4. Keller, Karen Laszlo, et al. Uses of vitamins A, C, and E and related compounds in dermatology: a review. *Journal of*

the American Academy of Dermatology, 39, 611-625 (1998).

5. Pinnell, Sheldon R. Cutaneous photodamage, oxidative stress, and topical antioxidant protection. *Journal of the American Academy of Dermatology*, 48, 1-22 (2003).

6. Xiao, Li, et al. Cytoprotective effects of the lipoidic-liquiform pro-vitamin C tetraiso-palmitoyl-ascorbate (VC-IP) against ultraviolet-A ray-induced injuries in human skin cells together with collagen retention, MMP inhibition and p53 gene repression. *Journal of Cellular Biochemistry*, 106, 589-598 (2009).

7. Nikko Chemicals Co., Ltd.

8 Trade publication "https://www.chemical-navi.com/english/product_search/detail389.html"

9. Luckewicz, Walter, et al. Determination of ascorbly dipalmitate in cosmetic whitening powders by differential scanning calorimetry. *Journal of the Society of Cosmetic Chemists*, 41, 359-367 (1990).

10. Lien, Mei-Hwa, Bin-Chung Huang, et al. Determination of ascorbyl dipalmitate in cosmetic whitening powders by liquid chromatography. *Journal of Chromatography A,* 645, 362-365 (1993).

11. Trade publication "https://www.chemical-navi.com/english/product_search/detail227.html"

12. Ochiai, Yasunobu, et al. A new lipophilic pro-vitamin C, tetra-isopalmitoyl ascorbic acid (VC-IP), prevents UV-induced skin pigmentation through its anti-oxidative properties. *Journal of Dermatological Science*, 44, 37-44 (2006).

13. Almeida, M. M., et al. Determination of tocopheryl acetate and ascorbyl tetraisopalmitate in cosmetic formulations by HPLC. *International Journal of Cosmetic Science*, 31, 445-450 (2009).

14. Liu, C., et al. Enhancement of dissolution of cyclosporine A using solid dispersions with polyoxyethylene (40) stearate. *Die Pharmazie-An International Journal of Pharmaceutical Sciences*, 61, 681-684 (2006).

15. Song, Jin-Deok, et al. Matrix-type transdermal drug delivery system and preparation method thereof. U.S. Patent No 8,404,277 (2013).

16. Palmer, Debbie M. Antioxidant skin care compositions. U.S. Patent No 8,361,520 (2013).

17. Cui, Chengji, et al. Stable topical compositions for 1, 2, 4-thiadiazole derivatives. U.S. Patent Application 13/835, 418 (2013).

作成日：2015 年 4 月 3 日

The Possible Role of RapGEF2 in CADM1 Overexpressed
Human Non-small Cell Lung Cancer
CADM1 を過剰発現させたヒト非小細胞性肺癌における RapGEF2 の役割の検討

研 究 者 氏 名　　　張　文静（第 36 期笹川医学研究者）

中国所属機関　　　山東省血液センター血液型研究室

日本研究機関　　　東京大学医科学研究所人癌病因遺伝子分野

指 導 責 任 者　　　村上　善則　教授

共同研究者名　　　松原大祐　講師，許淑真

Abstract:

Objective: Cell adhesion molecule 1 (CADM1) has been identified as a tumor suppressor in many human tumors including non-small cell lung cancer (NSCLC). The expression of CADM1 is lost in most of the lung cancer cell lines, however, in some specific lung cancer cells, CADM1 still maintains high expression. Our previous study found that RapGEF2 showed high co-expression with CADM1 in some specific lung cancer cells. Thus the present study is to investigate the possible roles of RapGEF2 in CADM1 overexpressed human non-small cell lung cancer.

Methods: Transwell migration assay and active Rap1 pull-down assay were performed in H1838 cells to detect the roles and mechanism of CADM1 and RapGEF2 in tumor migration, with or without knocking down CADM1 and RapGEF2 respectively. The survival assay was conducted to analyze the roles of CADM1 and RapGEF2 in patient prognosis.

Results: The cell migration was significantly suppressed after knocking down RapGEF2, while merely knocking down CADM1 had no significant influence on tumor cell migration compared to the control cells. Besides, the cell migration showed no significant difference in the presence of RapGEF2 with or without the expression of CADM1, while in the absence of RapGEF2, the cell migration was remarkably inhibited with CADM1 expression. Accordingly, the Rap1 activity was significantly decreased when RapGEF2 expression was blocked. Patients with high CADM1 expression showed better prognosis than the low expression group in the absence of RapGEF2, however, high CADM1 expression played no significant role in the prognosis with the presence of RapGEF2.

Conclusion: The present study indicated that RapGEF2 may play an oncogenic role in CADM1 overexpressed NSCLC cells.

Key words:

CADM1, RapGEF2, Rap1, NSCLC, adhesion, migration.

Introduction:

Lung cancer is the leading cause of cancer death in many developed countries, including the United States and Japan [1]. The cell adhesion molecule 1 (CADM1) has previously been identified as a tumor suppressor in human non-small cell lung cancer (NSCLC) [2]. Being involved in mediating cell-cell adhesion in calcium-independent manner, CADM1 is also involved in epithelial cell structure, as suppression of CADM1 in HEK293 by siRNA results in loosing of epithelial-like structure and changing to flat morphology of cells with immature cell adhesion patterns [3]. Goto et al has pointed out that in lung cancer cells, loss of CADM1 expression was associated with lower patient

survival [4]. They discovered that although CADM1 lost its expression in most of the lung cancer cells, it was still highly expressed in some particular cancer cells. And the mechanism of CADM1 actions in such cancer cells is still unclear.

Our previous study found through microarray assay that, in some lung cancer cell lines, Rap-specific Guanine Nucleotide Exchange Factor 2 (RapGEF2) indicated a strong co-expression with CADM1. RapGEF2 is a member of the RAS subfamily, specifically activating Rap1 by GTP-bounding. RapGEF2 is involved in the development of the neuronal migration [5]. In recent years, Rap1, which is a member of the RAS subfamily, has been found to be associated with many tumors, including melanoma, prostate cancer, thyroid tumor and breast cancer [6-9]. Rap1 localizes at the junctions in epithelial and endothelial cells to regulate cell-cell adhesion and cell-extracellular matrix adhesion [10]. Both CADM1 and Rap1 are involved in mediating the adhesion process, which is the key step for tumor development. An increase or decrease in the adhesion of tumor cells to neighboring tumor or host cells, extracellular matrix and endothelial cells may occur at different stages of tumor development and progression [11]. Till now, the role of RapGEF2-Rap1 signaling pathway in human lung cancer is still unclear.

The objective of the present study is to investigate the possible roles of CADM1 and RapGEF2 in human non-small cell lung cancer. We found that CADM1 expression may suppress the tumor cell migration with the absence of RapGEF2; besides, the cell migration could be significantly suppressed by knockdown of RapGEF2, possibly by decreasing Rap1 activity, yet still other mechanisms could not be excluded. Furthermore, the patient prognosis is much better with the presence of CADM1 expression in the RapGEF2 negative group.

Materials and Methods:

Protein expression profile of 41 non-small cell lung carcinoma (NSCLC) cell lines: We used the microarray analysis data of 41 cell lines, including 35 adenocarcinoma cell lines(H23, H292, H358, H441, H522, H596, H650, H1395, H1648, H1650, H1651, H1703, H1781, H1793, H1838, H1975, H1993, H2009, H2087, H2228, H2405, HCC827, HCC4006, Calu-3, A549, ABC-1, PC3, PC9, VMRC-LCD, RELF-LC-Ad1, RELF-LC-Ad2, HLC-1, LC-2/ad, RERF-LC-KJ, and L27), 4 large cell carcinoma cell lines (Lu65, H460, H661, and H1299), and one adenosquamous cell carcinoma cell line (H596)

Cell lines and antibodies: The H1838 cells were maintained in RPMI 1640 with 10% fetal bovine serum (FBS) and 1% antibiotics in a humidified atmosphere with 5% carbon dioxide and 95% air. The antibodies used in this study were summarized in Supplementary Table 1.

RNA interference studies: The siRNA oligonucleotides targeting CADM1 was (5' to 3'): CTGGCCCTATTTAGATGATAA. The siRNA sequences targeting RapGEF2 were synthesized by Invitrogen. The sequence of RapGEF2-#1 was (5'to3'): AUG UUU CCU GGU UAA UGA C.

Western blotting analysis: Cells were grown to confluence, collected, and then lysed with the lysis buffer. Supernatants were collected and protein concentrations were measured using the Bio-Rad protein assay. Samples were denatured, applied to an acrylamide gel followed by electrophoresis, and then transferred onto a PVDF membrane. The membrane was blocked in 3% skimmed milk solution or 5% Bull Serum Albumin (BSA), and was incubated firstly with specific antibodies and then with secondary antibodies. Protein bands were visualized using enhanced chemiluminescence with a protein-blotting detection method (GE Healthcare).

Rap1 activity assays: The levels of activated Rap1 were determined using pull-down assays with a glutathione S-transferase (GST) fusion of the Ras-binding domain of RalGDS. The Active Rap1 Pull-Down and Detection Kit was

from Thermo Scientific

Cell migration assay: The cell migration was analyzed by transwell migration assay. Briefly, after cells were transfected with siRNA for 72 h, cells were detached with trypsin, and 1×10^5 cells were placed into the upper chamber of the transwell, each chamber filled with 500 ul RPMI 1640 without FBS. The lower wells contained 750 ul of RPMI 1640 medium with 10% FBS. The cells were allowed to migrate for 24 h at 37℃ and the cells on the underside of the membrane were counted. Each sample was in triplicate.

Statistical analysis: Differences in mean values between the groups were analyzed by the Student's t-test. Disease-related survival was from the date of surgical resection to the date of death due to lung adenocarcinoma or the date when the patients were last known to be alive. Survival curves were estimated by the Kaplan-Meier method. $P<0.05$ was considered to be significant.

Results:

Expression pattern of CADM1 and RapGEF2 in 41 human lung cancer cell lines

Protein microarray analysis was conducted in 41 human lung cancer cell lines, and RapGEF2 showed a strong co-expression with CADM1 in several particular cell lines (Fig. 1). CADM1 has been identified as a tumor suppressor in NSCLC, and its expression was usually lost in most of the cancer cell lines, however, in some specific cell lines CADM1 still maintains high expression. The results indicated that RapGEF2, which co-expressed with CADM1 in some particular lung cancer cell lines, might have played some specific roles in lung cancer.

The roles of RapGEF2 and CADM1 in regulating cell migration in H1838 cells

As CADM1 has been identified as a tumor suppressor in NSCLC, the CADM1 expression is usually lost in tumor cells. However, in some tumor cells, CADM1 maintains high expression along with RapGEF2. In order to explore the possible roles of RapGEF2 and CADM1 in such lung cancer cell lines, the cells that express both CADM1 and RapGEF2 were selected. The H1838 cells were used to perform the transwell migration assay. RapGEF2 expression was silenced by siRNA, with or without knockdown of CADM1 (Fig. 2a). The results indicated that when RapGEF2 expression was blocked, CADM1 played a remarkable role in suppressing tumor cell migration; while in the presence of RapGEF2, the suppressive role of CADM1 in tumor migration was not significant (Fig. 2b).

These results suggested that RapGEF2 may play the role of stimulating tumor cell migration, and also may block the suppressive role of CADM1 in regulating tumor cell migration.

Rap1 activity was regulated by knockdown of CADM1 and RapGEF2:

As RapGEF2 could specifically activate Rap1, and Rap1 activation could mediate tumor cell migration and metastasis [6-8], it is interesting to investigate whether RapGEF2 regulates tumor cell migration through Rap1 activation. Active Rap1 Pull-Down Assay was performed in H1838 cells with or without knockdown of CADM1 and RapGEF2 (Fig.3a).The results showed that when RapGEF2 expression was blocked, Rap1 activity was significantly decreased compared with the control cells, and there was remarkable difference in Rap1 activity between CADM1 positive and negative groups (Fig. 3b). The results were in consistence with the transwell migration assay, which indicated that RapGEF2 may play the role of promoting cell migration through activating Rap1.

Roles of RapGEF2 and CADM1 in patient prognosis:

In order to analyze the roles of RapGEF2 and CADM1 in patient prognosis, we conducted the survival analysis. The patients were divided into RapGEF2 low-expression (n=223) and high-expression (n=220) groups. In RapGEF2 low expressed cases, the patients with high CADM1 expression (n=69) had significantly better prognosis than patients with

low CADM1 expression (n=154); while in RapGEF2 high expressed cases, CADM1 had no effect on the prognosis (Fig. 4). These results were in consistence with the migration assay, that the suppressive role of CADM1 in tumor cell migration may be inhibited by RapGEF2.

Discussion:

In the present study, we identified the possible roles of RapGEF2 in CADM1 high expressed lung cancer cells. In particular, we found that RapGEF2 may promote tumor cell migration possibly by activating Rap1; still, other mechanisms should not be excluded. Our data indicated that in the absence of RapGEF2, CADM1 high expression may inhibit tumor cell migration by blocking Rap1 activation, and the patient prognosis turned out to be significantly better than those with low CADM1 expression. With the presence of RapGEF2, the suppressive role of CADM1 in regulating cell migration was blocked, and Rap1 activity did not show any difference when CADM1 was knocked down compared with the control cells. Besides, the patient prognosis maintained the same between CADM1 high expression and low expression cases in the presence of RapGEF2.

Rap1 was first identified as a protein that could revert the morphologic phenotype of Ras-transformed cells, suggesting that Rap1 either mediated growth-inhibitory signals or interferes with Ras-effector signaling [12]. However, later studies suggested that Rap1 delivers an oncogenic signal, by which Rap1 could enhance cell adhesion and migration and activate survival pathways [13, 14]. In recent years, many studies have focused on the roles of Rap1 in cancers [6-9], and the results suggested that the roles of Rap1 in cancers are quite cell-specific. It may be partly because in tumor cells, Rap1 is activated by different stimulators. Although finally activating Rap1, different stimulators may exert different influences on cancer cells. Lyle et al has reported that Epac1-Rap1 signaling pathway could suppress cell migration in MDCK, A549 and RCC10 cell lines [15], while thrombin elicits a sustained increase in Rap1 activation, which is required for integrin signaling and proliferation of glioblastoma cells [16]. In addition, the various Rap1 downstream effectors may also lead to various outcomes. Thus, the roles of Rap1 in tumor cells depend on both cell types and environment context. By now, we are the first to examine the role of RapGEF2-Rap1 pathway in human lung cancer cells.

Loss of CADM1 expression has been reported in various cancers. In human lung adenocarcinoma cell line, A549, functional restoration of CADM1 expression could inhibit the tumor formation [17]. However, Goto et al found that in some specific lung adenocarcinoma subtypes, CADM1 maintains high expression [4]. What is the possible role of CADM1 in these subtypes? In the present study, RapGEF2 was found to co-express with CADM1 in some lung cancer cell lines, and RapGEF2-Rap1 signaling pathway may participate in the process. We suggest that RapGEF2 may inhibit the suppressive role of CADM1 in regulating tumor migration by activating Rap1. This result is not consistent with that in A549 cells [15], in which Rap1 activation could suppress cell migration, although both H1838 and A549 are lung cancer cell lines. One explanation is that there are different cell context and stimulators between the two cell lines. On one hand, CADM1 expression is lost in A549 cells, while it is highly expressed in H1838 cells; on the other, Epac-Rap1 instead of RapGEF2-Rap1 signaling pathway mainly elicits the downstream functions of Rap1 in A549 cells. Still, further study on RapGEF2-Rap1 signaling pathway in other cell lines should be encouraged.

In conclusion, the current study indicated the possible roles and mechanism of RapGEF2 in CADM1 highly expressed lung cancer cell lines. The RapGEF2-stimulated Rap1 activation was shown to contribute to cancer cells migration. In RapGEF2 high expression cases, the suppressive role of CADM1 in lung cancer was inhibited. Taken together, these data indicate that RapGEF2 may play an oncogenic role in human lung adenocarcinoma.

References:

1. Jemal A, Siegel R, Ward E, et al. Cancer statistics, 2006. CA: A Cancer Journal for Clinicians, 2006, 56:106-130.

2. Kuramochi M, Fukuhara H, Nobukuni T, et al. TSLC1 is a tumor-suppressor gene in human non-small-cell lung cancer. Nature Genetics, 2001, 27:427-430.

3. Sakurai-Yageta M, Masuda M, Tsuboi Y, et al. Tumor suppressor CADM1 is involved in epithelial cell structure. Biochemical and Biophysical Research Communications, 2009, 390:977-982.

4. Goto A1, Niki T, Chi-Pin L, et al. Loss of TSLC1 expression in lung adenocarcinoma: relationships with histological subtypes, sex and prognostic significance. Cancer Sci, 2005, 96:480-486.

5. Ye T1, Ip JP1, Fu AK, et al. Cdk5-mediated phosphorylation of RapGEF2 controls neuronal migration in the developing cerebral cortex. Nat Commun, 2014, 5:4826, doi: 10.1038/ncomms5826.

6. Gao L, Feng Y, Bowers R, et al. Ras-associated protein-1 regulates extracellular signal-regulated kinase activation and migration in melanoma cells: two processes important to melanoma tumorigenesis and metastasis. Cancer Res, 2006, 66:7880-7888.

7. Bailey CL, Kelly P, Casey PJ. Activation of Rap1 promotes prostate cancer metastasis. American Association for Cancer, 2009, DOI: 10.1158/0008-5472.CAN-08-4269.

8. Tsygankova OM1, Prendergast GV, Puttaswamy K, et al. Downregulation of Rap1GAP contributes to Ras transformation. Mol Cell Biol, 2007, 27:6647-6658.

9. Magliozzi R, Low TY, Weijts BG, et al. Control of epithelial cell migration and invasion by the IKKβ- and CK1α-mediated degradation of RAPGEF2. Dev Cell, 2013, 27:574-585.

10. Bos J.L. Linking Rap to cell adhesion. Curr. Opin. Cell Biol, 2005, 17:123-128.

11. Huang YW1, Baluna R, Vitetta ES. Adhesion molecules as targets for cancer therapy. Histol Histopathol, 1997, 12:467-477.

12. Kitayama H1, Sugimoto Y, Matsuzaki T, Ikawa Y, Noda M. A ras-related gene with transformation suppressor activity. Cell, 1989, 56:77-84.

13. Katagiri K, Maeda A, Shimonaka M, Kinashi T. RAPL, a Rap1-binding molecule that mediates Rap1-induced adhesion through spatial regulation of LFA-1. Nat Immunol, 2003, 4:741-748.

14. Bos JL. Linking Rap to cell adhesion. Curr Opin Cell Biol, 2005, 17:123-128.

15. Lyle KS, Raaijmakers JH, Bruinsma W, Bos JL, de Rooij J. cAMP-induced Epac-Rap activation inhibits epithelial cell migration by modulating focal adhesion and leading edge dynamics. Cell Signal, 2008, 20:1104-1116.

16. Sayyah J, Bartakova A, Nogal N, Quilliam LA, Stupack DG, Brown JH. The Ras-related protein, Rap1A, mediates thrombin-stimulated, integrin-dependent glioblastoma cell proliferation and tumor growth. J Biol Chem, 2014, 289:17689-17698.

17. Kuramochi M, Fukuhara H, Nobukuni T, et al. TSLC1 is a tumor-suppressor gene in human non-small-cell lung cancer. Nat Genet, 2001, 27:427-430.
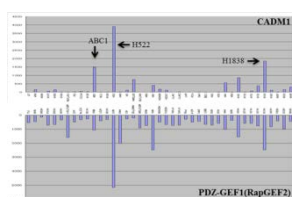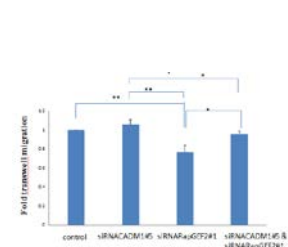
Fig.1   Fig.2a   Fig.2b

Figure1. RapGEF2 co-expressed with CADM1 in some lung cancer cell lines. Protein microarray assay was performed using 41 lung adenocarcinoma cell lines.

Figure 2. The roles of RapGEF2 and CADM1 in regulating tumor cell migration. (a) H1838 cells were transfected with siRNA RapGEF2 and siRNA CADM1 respectively, and the levels of RapGEF2 and CADM1 were tested by western blotting analysis 72 h later. (b) Transwell migration assay was perfomed in H1838 cells. After knockdown of RapGEF2 and CADM1 respectively, cells were placed into the upper chamber, and the cells migrated toward a lower chamber containing media with 10% FBS and were assessed after 24 h. The data represent results pooled from three independent experiments with at least three replicates each, and are plotted as te ratio of the number of migrated cells versus that of control cells. **, p<0.01; *, p<0.05.
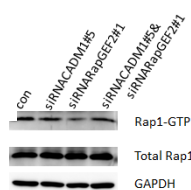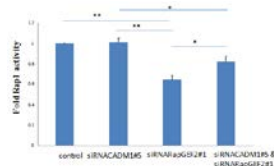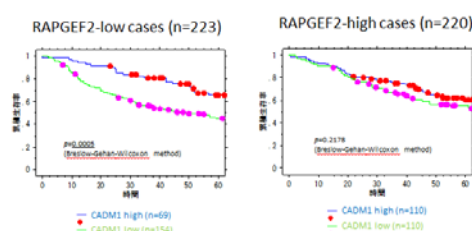

Fig.3a   Fig. 3b   Fig. 4

Figure 3. The roles of RapGEF2 and CADM1 in regulating Rap1 activity. (a) H1838 cells were transfected with siRNA RapGEF2 and CADM1. The cell lysates were analyzed in a pull-down assay using a GST fusion of the activated Rap1-bingding domain of RalGDS. The levels of precipitated Rap1 were determined by western blotting analysis using an anti-Rap1 antibody. Levels of Rap1-GTP, total Rap1 and GAPDH were detected by western blotting analysis. Data are from a single experiment that is representative of three separate experiments. (b) Data are plotted as the ratio of the amount of Rap1-GTP versus that of total Rap1. The data represent results pooled from three independent experiments. **, p<0.01; *, p<0.05.

Figure 4.The survival curves according to RapGEF2 and CADM1 expression. Patients were classified into two groups according to their RapGEF2 expression: RapGEF2-low cases (n=223), and RapGE2-high cases (n=220). In each group, the prognosis was assessed between CADM1 high expression and low expression cases.

Supplementary Table 1: List of antibodies used in this study.

Antibody	Name	Company	Species	Purpose (Concentration)
RapGEF2	1E8	Abnova	Mouse mAb	WB (1:500)
CADM1	C18	MBL	Rabbit pAb	WB (1:10000)
Rap1		Thermo Scientific	Rabbit mAb	WB (1:1000)
GAPDH	6C5	Millipore	Mouse mAb	WB (1:10000)

WB: western blotting; mAb: monoclonal antibody; pAb: polyclonal antibody.

作成日：2015 年 4 月 9 日

Analysis of CD72 binding with sulfated glycans
CD72 分子と結合する糖鎖リガンドの機能の解析

研 究 者 氏 名　　　劉　志紅（第 36 期笹川医学研究者）

中国所属機関　　　中国医科大学附属第一病院

日本研究機関　　　東京医科歯科大学難治疾患研究所

指 導 責 任 者　　　鍔田　武志　教授

共同研究者名　　　赤津ちづる　助教

Abstract:

In B cells (B lymphocytes), the B-cell receptor (BCR) co-receptor CD72 functions as a negative regulator of BCR signaling, and the polymorphism of CD72 is associated with autoimmune diseases. CD72 contains C-type lectin-like domain (CTLD) in its extracellular domain although the lectin activity had not been demonstrated. Recently the study in our laboratory showed that CD72 had a lectin activity to several sulfated ligands using glycan array technique. In this study, we aimed to clarify the binding ability of CD72 with sulfated glycans.

The recombinant Avi- and His-tagged CTLD of CD72 protein was expressed using Escherichia coli (E. coli) expression technique. As the protein was divided in inclusion bodies, the expressed protein was denatured. To make the protein functional, the denatured protein was refolded by on-column refolding technique and purified by affinity chromatography using His-tag binding beads. The recombinant protein was used to examine binding activity to various glycans (dextran sulfate, dextran, heparin, chondroitin sulfate A/B/C and hyaluronan) by ELISA. Among the glycans examined, heparin and chondroitin sulfate B showed strong binding with CD72 protein, and CD72a showed higher binding with these two ligands than CD72c.

Then, to investigate biological function of interaction between CD72 and glycan ligand, WT and CD72KO mice were immunized with platelet factor 4 (PF4)/heparin complex and antibody production against the complex was examined. Heparin-induced thrombocytopenia (HIT) is a life-threating thrombotic disease caused by antibodies to the complex consisting of heparin and PF4. As CD72 showed binding activity to heparin, we hypothesized that CD72 binded to heparin and inhibited production of anti-PF4/heparin antibodies.

First the recombinant PF4 protein was prepared using E coli expression methods, then the WT and CD72KO mice were immunized with PF4/heparin complex by intravenous retro-orbital (IV-RO) or intraperitoneal (IP) injection. We immunized the mice under several conditions, but unfortunately none of the mice immunized showed antibody production against PF4/heparin in this study.

Taken together, we revealed that CD72 CTLD had binding affinity to several sulfated glycan *in vitro*. The biological function of interaction between CD72 and glycan ligand is under investigation.

Key Words:

B cell, CD72, sulfated glycan, heparin induced thrombocytopenia

Introduction:

B cells are a type of lymphocytes playing an important role in the humoral immunity of the adaptive immune system. B cells are distinguished from other lymphocytes like T cells and NK cells by the presence of B-cell receptor (BCR) and ability of antibody production. When B cells interact with antigens, BCR mediates signal transduction that triggers antigen recognition (1). Several co-receptors located on the B-cell surface modulate this BCR signaling positively or negatively (2). CD72 is a 45-kDa type II membrane protein expressed on the surface of B cells and known to be negative regulator of BCR signaling. CD72 contains a C-type lectin-like domain (CTLD) in the extracellular region (3), and recently we revealed that the CTLD domain had lectin activities especially to sulfated glycans using glycan array technique. Therefore we hypothesized that inhibitory activity of CD72 to BCR signaling was regulated by glycan

ligands so that CD72 was responsible for the control of immune response against sugar ligands in some autoimmune.

In the current study, recombinant protein of CD72 CTLD was prepared and the reactivity of the recombinant protein to several glycans were examined by ELISA. Then to investigate whether autoantibody production against heparin, a kind of sulfated glycan, was regulated by CD72 *in vivo* or not, WT and CD72 deficient (CD72KO) mice were immunized with a mixture of heparin and platelet factor 4 (PF4) and antibody production was analyzed

Methods:

Purification of Avi-and His-tagged mouse CD72CTLD protein

The expression plasmid for production of Avi- and His-tagged CD72CTLD was prepared previously in our laboratory. Escherichia coli (E coli) cells containing the biotin ligase (birA) gene on a plasmid, BL21AI-BirA, was transformed with the expression plasmid and the transformants were cultured in LB medium containing 30 μg/mL kanamycin and 10 μg/mL chloramphenicol. When the optical density (OD) at 600 nm reached to 0.4, protein expression was induced by 1 mM IPTG and 0.2 % arabinose in the presence of 50 μM D-biotin for 12 hours at 18 °C. During the protein induction, both BirA and AviHisCD72CTLD proteins were allowed to be co-expressed and AviHisCD72CTLD was subsequently biotinylated by BirA.

The cells were then harvested and suspended in lysis buffer (50 mM Tris-HCl (pH 8.0) containing 150 mM NaCl, 0.5 % TritonX-100, and 2 mM DTT) and sonicated on ice. After washing with lysis buffer without TritonX-100, the inclusion bodies were suspended in denaturing buffer (50 mM Tris-HCl (pH8.0) containing 6 M guanidine-HCl and 150 mM NaCl) and sonicated on ice. After addition of 40 mM DTT, the suspension was incubated at 37 °C overnight to denature misfolded structure completely and to reduce mismatched disulfide bounds. The suspension was then centrifuged and the supernatant filtered with 0.8 μm pore-size membrane was mixed with histidine binding beads (His-accept beads, Nacalai tesque) for 45 min at 4 °C. The mixture was applied onto chromatography column and refolded by passing through the refolding buffer (50 mM Tris-HCl (pH 8.0) containing 150 mM NaCl, 400 mM sucrose, 400 mM L-arginine, 5 % glycerol, 5 mM reducd-glutathione, and 0.5 mM oxidized-glytathione). Then the AviHisCD72 CTLD proteins were eluted with elution buffer (50 mM phosphate buffer (pH 8.0) containing 300 mM NaCl and 250 mM imidazole) from the beads. The eluted protein was analyzed by SDS-PAGE (12 % acrylamide gel) followed by staining with CBB G250.

Purification of mouse PF4 protein

The plasmid for producing mouse PF4 protein (mPF4), pT7-7 vector containing mouse PF4 gene was introduced into an E coli strain, BL21(DE3), by heat shock methods and the transformed cells were cultured in LB medium in a presence of 100 μg/mL ampicillin and 1 mM IPTG at 18 °C for 20 hours to induce mPF4 protein expression. The harvested cells were suspended in sonication buffer (50 mM Tris-HCl (pH8.0) containing 1 mM EDTA, 50 mM NaCl, 100 μg/mL lysozyme, 1 mM PMSF, and 0.5 % sodium deoxycholate) and sonicated on ice. Then 0.1 % TritonX-100 was added and incubated at 4 °C for 1 hour. After insoluble materials were removed by centrifugation, the supernatant was mixed with heparin-agarose beads (Sigma-Aldrich) at 4 °C overnight. The mixture was loaded onto the chromatography column and mPF4 protein was eluted with elution buffer (10 mM Tris-HCl (pH8.0) containing 1 M NaCl). The eluted protein was analyzed by SDS-PAGE (15 % acrylamide gel) followed by CBB staining.

ELISA

For analysis of binding affinity of CD72 toward various glycan ligand, ELISA was performed as follows. 96-well ELISA plate (Greiner bio-one) was coated with 10 μg/ml Poly-L-Lysine (PLL) for 2 hours at room temperature (RT) and the 30 μg/ml of following glycans were immobilized on the PLL-coated plates; dextran sulfate, dextran, heparin, chondroitin sulfate A/B/C, or hyaluronan. After blocking with 1 % BSA-PBS (PBS containing 1 % BSA) for 2 hour at RT, 50 μL of AviHisCD72CTLD proteins (0 μg/ml, 0.4 μg/ml, 0.8 μg/ml, or 2.5 μg/ml) were added and incubated for 1 hour at RT. Plates were then washed three times with PBST (PBS containing 0.05 % Tween 20) and incubated with

alkali phosphatase (AP)-conjugated streptavidin (AP-SA) (BD Pharmingen). After washing three times with PBST, the enzymatic activity was detected using phosphatase substrate (Sigma-Aldrich) by measuring absorbance at 405 nm on a Vmax kinetic microplate reader (Molecular Devices).

To assess the antibody production in immunized mice, ELISA was carried out as follows. 10 μg/mL mPF4 or a mixture of 10 μg/mL mPF4 and 0.4 U /mL heparin were immobilized on the 96-well ELISA plate overnight at 4°C. After blocking with 1 % BSA-PBS, plates were incubated with mouse serum (diluted in 1 % BSA-PBS at 1:100) for 1 hour at RT. After three washes with PBST, the wells were incubated with AP-conjugated anti mouse IgG for 1 hour at RT, then the enzymatic activity of AP was detected as mentioned above.

Murine immunization

Wild-type C57BL/6 mice were purchased from Sankyo Laboratory Service (Tokyo, Japan) and CD72 deficient mice were generated previously in our laboratory and maintained under SPF conditions. For immunization with intravenous retro-orbital (IV-RO) injection, a mixture of 22 μg heparin and 40 μg mPF4 was dissolved in 100 μL Hank's balanced salt solution (HBSS) and administrated to the mice (10 weeks old) daily for 5 days or weekly for 3 weeks. For intraperitoneal (IP) immunization, 22 μg heparin and 40 μg mPF4 were mixed with 10 mg Alum (Aluminium Potassium Sulfate, Wako) and 100 μL mixture were injected to the mice. The first day of injection was considered day 0. Blood was collected at day -1 (before immunization) and day 14, day 21, day 28.

Results

Purification of AviHis CD72 CTLD protein

Recombinant mouse CD72CTLD protein tagged with Avi- and His-tag at N terminal was produced using E coli expression system. As expressed CD72CTLD protein was mainly divided in the inclusion bodies, the protein refolding was useful method to recover the proteins being structurally correct and functionally active. In this study, the AviHisCD72CTLD protein in the inclusion bodies was denatured and the denatured protein was refolded by on-column refolding technique. Then the refolded protein was eluted from the histidine binding beads and the recovered protein was analyzed by 12 % SDS-PAGE followed by CBB staining. As shown in Fig. 1, the refolded protein was obtained mainly as a monomer form (23 kDa), suggesting that the protein refolding was succeeded. The amount of the refolded proteins obtained from 1 L culture was approximately 0.3 mg as determined by Bradford assay.
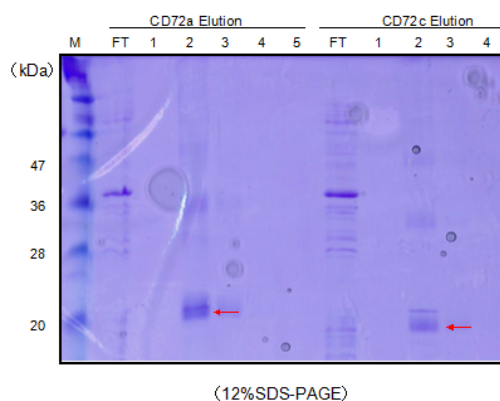

(12%SDS-PAGE)

Figure 1. Purification of recombinant AviHisCD72aCTLD and AviHisCD72cCTLD proteins.
The refolded proteins were eluted stepwise from His binding beads with 3 mL (0.6 mL x 5 fractions) elution buffer. Both CD72aCTLD and CD72cCTLD proteins were mainly recovered in fraction 2 as indicated by red arrows. M, molecular weight marker; FT, flow-through fraction.

Binding analysis of CD72 with sulfated glycans

In the previous study based on glycan array, the CD72CTLD showed binding affinity toward several sulfated glycans. To investigate the binding activities of recombinant CD72CTLD toward putative glycan ligands *in vitro*,

ELISA experiment was performed here. Several glycans were immobilized individually onto the PLL-coated microplate and then the CD72aCTLD or CD72cCTLD proteins were added to assess their binding activities toward immobilized glycans. PLL-coated wells without immobilization of any glycans were also prepared as a negative control (blank). Note that the CD72a and CD72c are the allelic variants of mouse CD72, and CD72c is known to be related to auto-immune disease. Significant bindings of both CD72aCTLD and CD72cCTLD proteins toward every glylcan ligand examined were observed in a dose dependent manner. Stronger bindings toward heparin and chondroitin sulfate B were observed in both CD72a and CD72cCTLD proteins. Compared to the reactivity toward chondroitin sulfate A, chondroitin sulfate C, hyaluronan, and dextran, CD72aCTLD reacted stronger to dextran sulfate. On the other hand, CD72cCTLD's reactivity to dextran sulfate was comparable level.
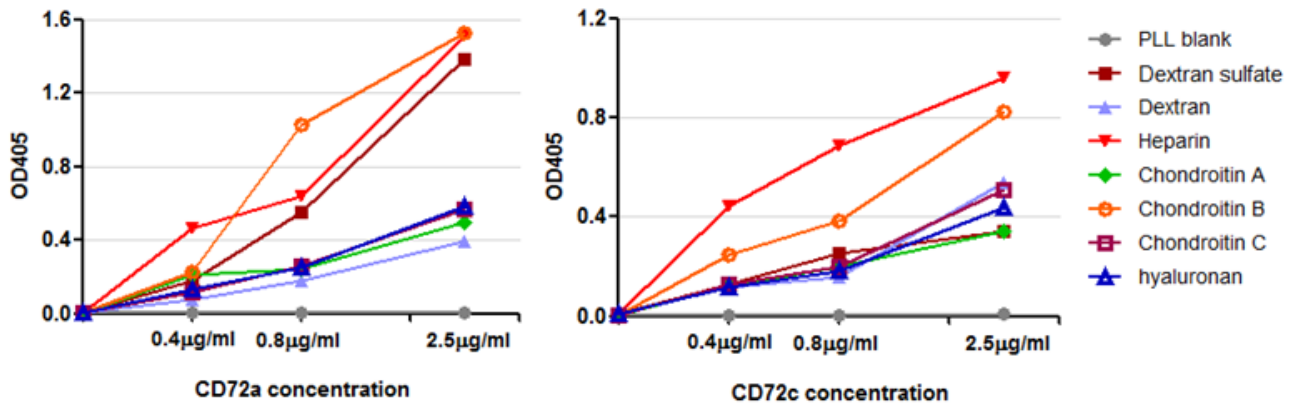

Figure 2. Binding affinity of CD72a and CD72c CTLD protein to various glycans

Effects of immunization

Heparin induced thrombocytopenia (HIT) is an acquired immune disorder and antibodies specific for PF4/heparin complexes are the central matter for its pathogenesis. As heparin showed strong binding to CD72CTLD protein in this study, we hypothesized that the production of pathogenic antibody against PF4/heparin was regulated by CD72 *in vivo*. Based on the hypothesis, next we assessed antibody productions in WT and CD72KO mice, both of which were immunized with mPF4/heparin complex.

First of all, the recombinant mPF4 protein was prepared by E coli expression technique. Then the expressed mPF4 was extracted from the bacterial cells using sonication and TritonX-100, then purified using heparin-binding beads. The recovered mPF4 was analyzed by 15 % SDS-PAGE followed by CBB staining. As shown in Fig 3, monomer form of mPF4 (8.2 kDa) was clearly observed, suggesting that the protein was successfully purified. Based on Bradford assay, the recovered protein was approximately 0.8mg from 2 L culture.
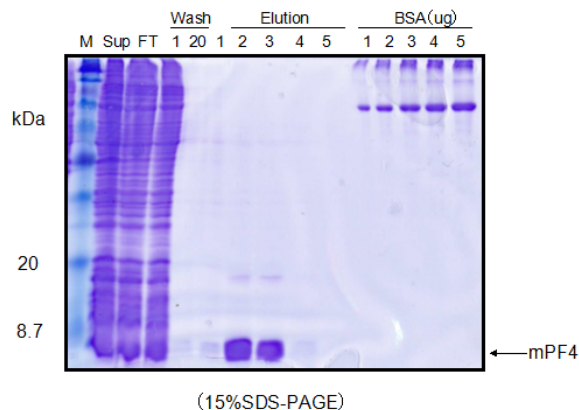

Figure 3. Purification of recombinant mouse PF4 protein.

The recombinant mPF4 proteins were purified by affinity chromatography using heparin-agarose beads. After washing the column with 20 mL washing buffer, mPF4 proteins were recovered with stepwise elution with 2.5 mL (0.5

mL x 5 fractions) elution buffer. The mPF4 protein was mainly eluted in fractions 2 and 3 as indicated by arrow. M, molecular weight marker; Sup, supernatant (unpurified sample fraction); FT, flow-through fraction.

The purified mPF4 protein was mixed with heparin at 200 μg/mL (mPF4) and 110 μg/mL (heparin) in HBSS and 100 μL of the mixture were injected to the mice via IV-RO daily for 5 days as described previously (4). Then the antibody against PF4/heparin was analyzed by ELISA using serum collected at 7-day interval after immunization. However no antibody production was observed in both WT and CD72KO mice (data not show). Therefore, to optimize the immunization methods, mice were administrated the mPF4/heparin under the several different conditions and antibody production was examined.

First, PF4 (20 μg/mouse) and heparin (11 μg /mouse) were mixed with adjubant, Alum (Aluminium Potassium Sulfate, Wako) (10mg/mouse), and the mixture was administrated to the WT and CD72KO mice by IP injection every two weeks. The serum samples were collected sequentially at day 14, day 28, day 42. Even after 6 weeks of the initial immunization, the antibody productions were not observed (data not shown). Next, two times higher amounts of PF4 and heparin, i.e. 40 μg/mouse of PF4 and 22μg /mouse of heparin, were mixed with or without Alum (10mg/mouse), then the mixture of PF4 and heparin was subjected to IV-RO immunization, and the mixture of PF4, heparin, and Alum was to IP immunization. The administration of the antigen was done weekly, and antibody productions were analyzed by ELISA using the serum at day 14, day 21, and day 28. Even though the mice were immunized with higher amounts of PF4 and heparin, either WT or CD72KO mice were not produce anti PF4/heparin antibodies (Fig 4). From these results, it is still unclear whether the CD72 regulates antibody production against heparin, a sulfated glycan. Further investigation is required.
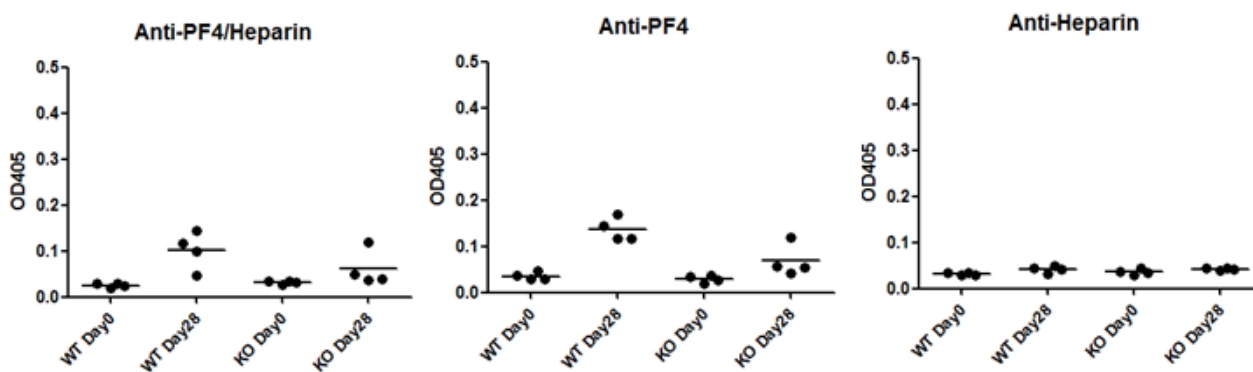

Figure 4 Anti-PF4/Heparin, anti-PF4 and anti-Heparin antibodies production (IV-RO immunization, a mixture of 22μg heparin and 40 μg mPF4 was dissolved in 100 μL HBSS, Blood was collected at day 28)

Discussion

CD72 is known as an inhibitory regulator of the BCR signaling and ligand binding activity is defined in the extracellular domain of CD72. CD100 has been identified as a natural ligand of CD72 and reported to regulate BCR signaling by turning off negative signaling by CD72 (5). The ligand of CD72 may have a critical role in controlling BCR signaling by regulating CD72's activity.

CD72 has CTLD in its extracellular domain, suggesting that CD72 may be controlled by its glycan ligands. However, because the CTLD lacks typical Ca^{2+} binding site, which is conserved in general C-type lection, the lectin activity of CD72's CTLD had been unclear for a long time. Recently we revealed that the CTLD had binding activity to sulfated glycans (unpublished data). In this study, to clarify the role of glycan ligand to exert regulatory effect of CD72, recombinant CD72CTLD protein was prepared and the binding affinity of the protein to several glycan ligands was analyzed by ELISA.

First, we prepared recombinant mouse CD72a CTLD and D72c CTLD proteins. In mouse, four allelic variants of CD72, (CD72a, CD72b, CD72c, and CD72d) were defined. Among the four, CD72c has a marked difference in CTLD domain; 7-AA lacks in CTLD of CD72c although the AA sequences in other regions are identical to those of the other

alleles. CD72c isoform has also been demonstrated to association with autoimmune disease (6). Therefore we also compared binding activities of CD72a and CD72c CTLDs to sulfate glycans.

Among the sulfated glycans tested here, dextran sulfate, heparin, and chondroitin sulfate B showed stronger reactivity to CD72 CTLD. Compared to CD72a CTLD, CD72c CTLD's binding activity to the three glycans was slightly reduced, suggesting that CD72c had weaker binding activity to the glycan ligands. The regulation by glycan ligand might be modified in CD72c and it might be associated with autoimmune disease.

In immune system, the B cell maturation undergoes programmed cell death, and results in B cell differentiation into antibody-producing cells. Thus, the signal which blocks the death of B cells is required for activation of B cells. The previous study demonstrated that dextran sulfate prevented B cells from cell death (7). Therefore, the interaction of CD72 and dextran sulfate may be a biologically meaningful event. In addition, chondroitin sulfate B also showed specific binding to CD72 CTLD, but chondroitin A/C showed weak binding with CD72 CTLD. Chondroitin sulfate (CS), which belongs to the glycosaminoglycan (GAG) superfamily, is a linear sulfated polysaccharide involved in various biological processes. CS structure is very heterogeneous and contains various sulfation patterns owing to the multiple and random enzymatic modifications that occur during its biosynthesis (8). It was maybe the reason why CD72 CTLD binds to chondroitin sulfate B specifically.

As described above, mPF4/heparin complex is an auto-antigen in HIT. As heparin showed strong binding affinity to CD72 CTLD, we hypothesized that in HIT CD72 might be preventing auto-antibody production against PF4/heparin complex in healthy individuals. To confirm this hypothesis, WT mice and CD72KO mice immunization experiments were studied. However, the antibody production against PF4/heparin was not observed in either WT or CD72KO mice in this study maybe because PF4/heparin had low immunogenicity. Further investigation should be required under modified immunization conditions.

In this study, we produced recombinant mouse CD72CTLD proteins and revealed that CD72CTLD has binding activities to several sulfated glycans *in vitro*. This is first report to show the lectin activity of CD72CDLD domain toward several sulfated glycans.

References

1. Tsubata, T., and Wienands, J. B cell signaling. Introduction. Int Rev Immunol. 20, 675-678 (2001).

2. Fujimoto, M., and Sato, S. B cell signaling and autoimmune diseases: CD19/CD22 loop as a B cell signaling device to regulate the balance of autoimmunity. J Dermatol Sci. 46, 1-9 (2007).

3. Adachi, T., H. Flaswinkel, H. Yakura, M. Reth, T. Tsubata. The B cell surface protein CD72 recruits the tyrosine phosphatase SHP-1 upon tyrosine phosphorylation. J. Immunol. 160: 4662–4665. (1998)

4. Suvarna S., Qi R., Arepally GM. Optimization of a murine immunization model for study of PF4/Heparin antibodies. J Thrombosis Haemostasis 2009; 7, 857-864. (2009)

5. Kumanogoh, A., Watanabe, C., Lee, I., Wang, X., Shi, W., Araki, H., Hirata, H., Iwahori, K., Uchida, J., Yasui, T., Matsumoto, M., Yoshida, K., Yakura, H., Pan, C., Parnes, J. R., and Kikutani, H. Identification of CD72 as a lymphocyte receptor for the class IV semaphorin CD100: a novel mechanism for regulating B cell signaling. Immunity. 13, 621-631 (2000).

6. Miduo Xu., Rong Hou., Aya Sato-Hayashizaki., Rongyong Man., Chenghua Zhu., Chisato Wakabayashi., Sachiko Hirose., Takahiro Adachi and Takeshi Tsubata. Cd72c is a modifier gene that regulates Fas[lpr]-induced autoimmune disease. J. Immunol. 190: 5436–5445 (2013)

7. Nomura, T., Han, H., Howard, M. C., Yagita, H., Yakura, H., Honjo, T., and Tsubata, T. Antigen receptor-mediated B cell death is blocked by signaling via CD72 or treatment with dextran sulfate and is defective in autoimmunity-prone mice. Int Immunol. 8, 867-875 (1996).

8. Wakao, M., Obata, R., Miyachi K., kaitsubata Y., Kondo T., Sakami C., Suda Y.Synthesis of a chondroitin sulfate disaccharide library and a GAG-binding protein interaction analysis. Bioorg Med Chem Lett. 1407-1411 (2015).

作成日: 2015 年 4 月 7 日

Characterization of self-assembled virus-like particles of dromedary camel hepatitis E virus generated by recombinant baculoviruses

組換えバキュロウイルス発現システムを用いたラクダ由来 E 型肝炎ウイルス様粒子の作製

研 究 者 氏 名　　　周　顕鳳（第 36 期笹川医学研究者）

中国所属機関　　　南昌市疾病予防コントロールセンター微生物科

日本研究機関　　　日本国立感染症研究所ウイルス第二部

指 導 責 任 者　　　李　天成　　主任研究官

Abstract:

Dromedary camel hepatitis E virus (DcHEV), a novel hepatitis E virus, has been identified in dromedary camels in Dubai, United Arab Emirates. The antigenicity, pathogenicity and epidemiology of this virus have remained unclear. In the present study, we first used a recombinant baculovirus expression system to express the 13 and 111-N-terminus amino-acid-truncated DcHEV ORF2 protein in insect Tn5 cells, and obtained two kinds of virus-like particles (VLPs) with densities 1.300 g/cm^3 and 1.285 g/cm^3, respectively. The small VLPs (Dc4sVLPs) were estimated to be 24 nm in diameter, were assembled by the protein with molecular weight 53 kDa, and large VLPs (Dc3nVLPs and Dc4nVLPs) in diameter 35 nm composed of protein with 64 kDa. Antigenic analysis demonstrated that DcHEV was cross-reactive with G1, G3-G6, ferret and rat HEVs, and DcHEV showed a stronger cross reactivity to G1 and G3-G6 HEV than it did to rat and ferret HEV. Furthermore, the antibody against DcnVLPs neutralizes G1 and G3 HEV, suggesting that the serotypes of these HEVs are identical. In addition, we found that the amino acid residue Met-358 affect the DcsVLPs assembly.

Keywords:

Dromedary camel HEV; Recombinant baculovirus; Virus-like particles, Insect cells Tn5

Introduction

Hepatitis E virus (HEV) is causative agent of hepatitis E, a viral disease that manifests as acute hepatitis E (Emerson and Purcell 2003). The HEV infection occurs mainly through the fecal-oral route (1), and acute hepatitis E is known as an important public health problem not only in developing countries but also in industrialized countries, there the HEV was mainly transmitted by imported or zoonotic infection (2). HEV, a small non-enveloped single-stranded, positive-sense RNA virus, is classified as the sole member of the genus *Hepevirus* in the family *Hepeviridae*. The genome of HEV is approximately 7.2 kilobases (kb) in size, and contains three open reading frames (ORFs). ORF1 encodes non-structural proteins involved in replication and viral protein processing. ORF2 encodes a capsid protein that contains immunogenic epitopes, induces neutralizing antibodies, and is the target for vaccine development. ORF3, which partially overlaps with ORF2, encodes a cytoskeleton-associated phosphoprotein with multiple functions.

To date, at least 4 genotypes of HEV that infect humans have been identified. A number of sporadic cases have been transmitted in a zoonotic fashion in developed countries, with zoonotic hepatitis E being mainly associated with genotype 3 or 4 HEV infections (3).

Dromedary camel HEV (DcHEV), a brand-new HEV was first identified from fecal samples of dromedary camels (*Camelus dromedarius*) in 2013 in Dubai, United Arab Emirates (4). Complete genome sequencing of two DcHEV

strains showed more than 20% overall nucleotide difference to known HEVs, and only shared 52.1-56.5% nucleotide identity with avian, bat, rat and ferret HEVs. While the genome has been sequenced, the antigenicity, pathogenicity and epidemiology of DcHEV have remained unclear because of the lack of a cell-culture system to grow the virus.

In this study, we describe the efficient expression of 13- or 111-N-terminus-aa-deleted DcHEV ORF2 proteins by a recombinant baculovirus in insect Tn5 cells, the proteins were found to self-assemble into virus-like particles (VLPs). The VLPs exhibited antigenic cross-reactivity with rat, ferret, G1 and G3 to G6 HEVs and the serotype of DcHEV was identical to G1 and G3 HEV.

Materials and Methods

Construction of transfer vectors. Two full-length ORF2 of the DcHEV containing the *Bam*HI site before the start codon and the *Xba*I site after the stop codon were synthesized based on the DcHEV sequence deposited in GenBank (KJ496143 and KJ496144). For simplicity, we proposed Dc3 (KJ496143) and Dc4 (KJ496144) as these two DcHEV strains' numbers in this study, respectively. These full-length ORF2s were cloned into a vector, pUC57, to generate a plasmid, pUC57-Dc3ORF2 and pUC57-Dc4ORF2 (GeneScript, Piscataway, NJ), respectively. DNA fragments encoding the N-terminus-truncated DcHEV ORF2s were amplified by PCR using plasmid pUC57-Dc3ORF2 or pUC57-Dc4ORF2 as a template. The DNA fragments encoding 13- and 111-N-terminal-aa-truncated DcHEV ORF2s were amplified by PCR with the primers, DcHEV-N13 (5'-AAGGATCCATGTTGCCTATGCTGCCCGCGCCA-3') /DcHEV-CR1 (5'-AGTCTAGATTAATACTCCCGAGTTTTACCCA-3'), and DcHEV-N111 (5'-AAGGATCCATGGCTGTTGCTCCCGCCCCAGG-3') /CR1, respectively. The full-length and truncated ORF2s were digested with *Bam*HI and *Xba*I, and ligated with a baculovirus transfer vector, pVL1393 (Pharmingen, San Diego, CA), to yield plasmids pVL1393Dc3ORF2, pVL1393Dc3n13ORF2, VL1393Dc3n111ORF2, VL1393Dc4ORF2, pVL1393Dc4n13ORF2, pVL1393Dc4n111ORF2. Mutation were introduced by PCR amplification of overlapping fragments with specifically mutated primers DcHEV-n111/Dc3ORF2-358R (5'-TAGACCATTCGTACCAGTAAA-3'), and Dc3ORF2-358F (5'-TTTACTGGTACGAATGGTCTA-3')/CR1, by using the pUC57-Dc3ORF2 as a template. Consequently both fragment were purified and combined in a fusion PCR with the primers DcHEV-n111/CR1. Finally, this fragment was cloned into transfer vector, pVL1393 to yield plasmid pVL1393Dc3n111ORF2mt.

Construction of a recombinant baculovirus and expression of capsid proteins. Sf9 cells were co-transfected with a linearized wild-type *Autographa californica* nuclear polyhedrosis virus DNA and transfer plasmids by a lipofectin-mediated method. The cells were incubated at 26.5°C in TC-100 medium supplemented with 8% fetal bovine serum and 0.26% tryptose phosphate broth. The recombinant viruses were plaque-purified in Sf9 cells and designated as Ac[Dc3ORF2], Ac[Dc3n13ORF2], Ac[Dc3n111ORF2], Ac[Dc4ORF2], Ac[Dc4n13ORF2], Ac[Dc4n111ORF2], and Ac[Dc3n111ORF2mt]. Tn5 cells were infected with recombinant baculoviruses at a multiplicity of infection (MOI) of 10.

SDS-PAGE and Western blot assay. The proteins in the cell lysates and culture medium were separated by 5-20% SDS-PAGE and stained with Coomassie blue (CB). For the Western blot analysis, proteins in the gel were electrophoretically transferred onto a nitrocellulose membrane. The membrane was then soaked with 5% skim milk in 50 mM Tris-HCl (pH 7.4), 150 mM NaCl, and incubated with rabbit anti-G1 HEV-LPs polyclonal antibody. Detection of the rabbit IgG antibody was achieved using alkaline phosphatase-conjugated goat anti-rabbit immunoglobulin (1:1000 dilution). Nitroblue tetrazolium chloride and 5-bromo-4-chloro-3-indolyl phosphate P-toluidine were used as coloring agents.

Purification of VLPs and transmission electron microscopy (TEM). The recombinant baculovirus-infected Tn5 cells were harvested on day 7 post-infection (p.i.). After removed the intact cells, cell debris, and progeny baculoviruses by centrifugation at 10,000 g for 60 min, the supernatant was then spun at 32,000 rpm for 3 h, and the resulting pellet was resuspended in EX-cell 405 medium at 4°C overnight. The recombinant baculovirus infected cells were treated and purified as previously reported (5). Purified VLPs were placed on a carbon-coated grid for 45 seconds, rinsed with distilled water, stained with a 2% uranyl acetate solution and examined with a JEOL TEM-1400 electron microscope operating at 80 kV.

Structural observation. The atomic structure of T=1 particle (PDB-id: 2ztn) and pseudo-atomic structure of T=3 particle (PDB-id: 3iyo) are both downloaded from PDB database. The measurements of the distance of residues were performed by Pymol software and the figures were made by use of the software UCSF Chimera.

N-terminal amino acid sequence analysis. The proteins were purified by CsCl gradient centrifugation. The N-terminal aa microsequencing was carried out using 100 pmol of protein by Edman automated degradation on an Applied Biosystems model 477 protein sequencer.

Hyperimmune sera and detection of anti-HEV IgG antibody. Rats (Wistar, 12 weeks old, female) were immunized with Dc3nVLPs. The immunization was performed with thigh muscle injection of purified VLPs with a dose of 200 µg per rat, and booster injections were carried out at 4 and 6 weeks after the first injection with half doses of VLPs. Immunized animals were bled one week after the last injection. ELISA for detection of anti-HEV IgG was performed with purified recombinant HEV virus-like particles (VLPs) (1 µg/ml, 100 µl/well) (5).

Cell culture-based neutralizing activity test. Infectious G1 and G3 HEV strain (G3-HEV83-2-27, GenBank no. AB740232) were used to evaluate the neutralizing activity of anti-HEVs antibodies. HEV grows in PLC/PRF/5 cells and is efficiently released to cell culture supernatants. Pre- and post-HEV-LPs-immunized rat serum and rat HEV-infected rat serum were heated at 56°C for 30 minutes and then diluted to 1:10 and 1:100 with medium 199. One mililiter of the solution containing 2×10^6 copies of G1 or G3 HEV was mixed with 1ml of diluted antiserum and incubated at 37°C for 1hr, and then at 4°C for 3 hrs. A hepatocarcinoma cell line, PLC/PRF/5, was cultured in 6-well cell culture plates (5×10^5 cells/well) with 5 ml DMEM containing 10% (v/v) heat-inactivated FCS. One ml of the virus/serum mixture was added to each well of the plates, after removing the cell culture medium. After adsorption at 37°C for 1 hr, the cells were washed three times with PBS (-), and 4 ml maintenance medium consisting of medium 199 (Invitrogen, Carlsbad, CA), 2% (v/v) heat-inactivated FCS and 10 mM $MgCl_2$. The culture medium was replaced with new medium every 3 days. Neutralizing activity was monitored by detection of HEV Ag in the cell culture supernatant at three weeks post-inoculation by ELISA.

Results

Expression of DcHEV ORF2 and formation of virus-like particles

Six recombinant baculoviruses, Ac[Dc3ORF2], Ac[Dc3n13ORF2], Ac[Dc3n111ORF2], Ac[Dc4ORF2], Ac[Dc4n13ORF2], and Ac[Dc4n111ORF2] were prepared as described in the Methods section. Tn5 cells were infected with the recombinant baculoviruses at a multiplicity of infection (MOI) of 10, incubated at 26.5°C, and harvested every day up to day 10 post infection (p.i.). The proteins generated in the infected cells and supernatant were analyzed by SDS-PAGE. In Ac[Dc3ORF2] and Ac[Dc4ORF2]-infected Tn5 cells, major protein bands with molecular masses of 72

kDa corresponding to the full-length of ORF2 proteins were detected at 2 days p.i.. However, those proteins were not detected in the supernatant and no VLPs were observed in either the cells or their supernatants.
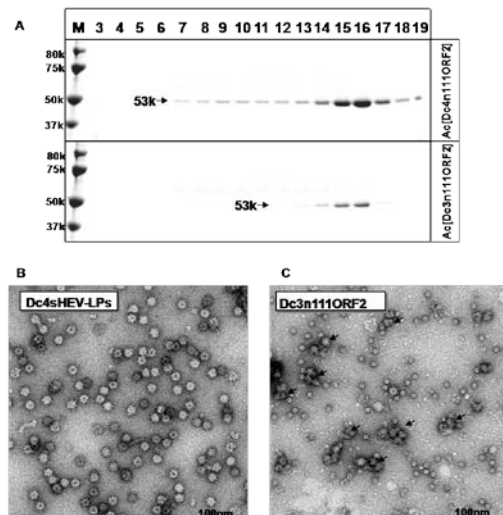
In the Ac[Dc3n111ORF2] and Ac[Dc4n111ORF2]-infected Tn5 cells, a major protein with a molecular mass of 58 kDa (D-p58) was detected in the cells from day 2 p.i., and a protein migrating with a molecular mass of 53 kDa (D-p53) was found in the cells and supernatant from day 4 p.i. The D-p58 protein was synthesized only in Ac[Dc3n111ORF2] and Ac[Dc4n111ORF2]-infected Tn5 cells and D-p53 protein was detected only in Ac[Dc3n111ORF2] and Ac[Dc4n111ORF2]-infected Tn5 cell culture supernatant, not in the mock-infected or wild-type baculovirus-infected cells. The 53kDa proteins reacted with anti-G1 HEV-LPs antibody in Western blots (Fig.1).
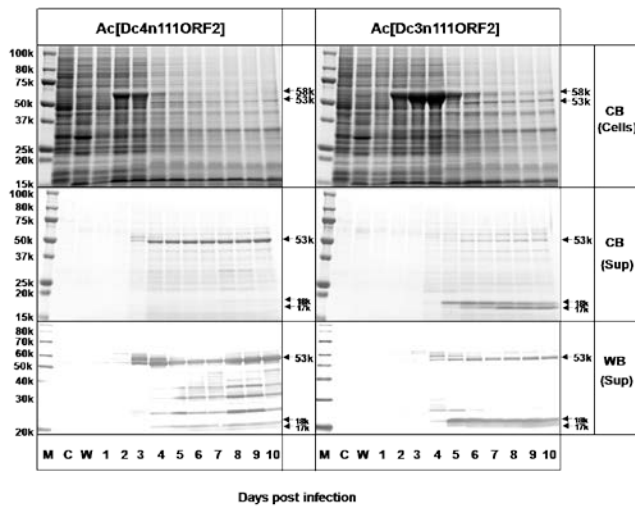
Fig. 1. Time course of the expression of 111-N-terminal aa-truncated DcHEV ORF2. Insect Tn5 cells were infected with a recombinant baculovirus Ac[Dc3n111ORF2] and Ac[Dc4n111ORF2], incubated at 26.5°C, and harvested on the indicated days (day 1 to 10).

Fig. 2. Purification of VLPs from cell culture. (A). To examine the VLPs, each fraction containing D-p53 protein was stained with 2% uranyl acetate and observed by EM: Dc4sVLPs (B) and aggregations of D-p53 proteins (C). Bar, 100 nm.

Comparing of the amount of D-p53 in supernatant we found that the D-p53 protein is larger in Ac[Dc4n111ORF2]-infected cell culture supernatant than that in Ac[Dc3n111ORF2]. Two small proteins with molecular weight about 17-18 kDa was clearly detected in Ac[Dc3n111ORF2]-infected cell culture supernatant by SDS-PAGE and these two proteins reacted with rabbit anti-G1 HEV-LPs antibody by western blotting, indicating that these two proteins were derived from Dc3 ORF2. These observed degraded proteins reveal that the D-p53 protein derived from Ac[Dc3n111ORF2] is unstable.

To examine whether the D-p53 protein would form VLPs, the cell culture supernatants of the Ac[Dc3n111ORF2] and Ac[Dc4n111ORF2]-infected Tn5 cells were harvested and subjected to CsCl gradient centrifugation. In the Ac[Dc4n111ORF2]-infected cell culture supernatant the D-p53 protein was mainly distributed in fractions 15 and 16 (Fig. 2A). Electron microscopy (EM) of fraction 15 and 16 showed many spherical particles with diameter of about 24 nm (Fig. 2B). In contrast, the D-p53 protein in Ac[Dc3n111ORF2]-infected Tn5 cell culture supernatant were found in fractions 15 and 16, and some aggregations of D-p53 proteins were observed by EM, however, no VLPs was found (Fig.2C). The N-terminal aa sequence of D-p53 indicated that D-p53 was derived from the DcHEV ORF2 protein and with ~50 aa deletion at the C-terminus. These results indicated that the D-p53 derived from Dc4 self-assembled into VLPs which smaller than native virus particle and were named as Dc4sVLPs.

In the Ac[Dc3n13ORF2] and Ac[Dc4n13ORF2]-infected Tn5 cells four major proteins with molecular mass of 40 kDa (p40), 53 kDa (D-p53) 64 kDa (D-p64) and 70 kDa (D-p70) were observed, respectively (Fig. 3A). Proteins D-p53, D-p64 and D-p70 were reacted with rabbit anti-G1 HEV-LPs Ab by western blot assay, indicating that these three proteins were derived from the DcHEV ORF2. In the cell culture supernatants only D-p53 was detected by SDS-PAGE with very thin band. To purify VLPs from cells, Tn5 cells were harvested at 7 days p.i., and treated with denature buffer. After CsCl gradient centrifugation, proteins, D-p64 mainly appeared in fractions 9 and 10 (Dc3) or 9 to 11 (Dc4) fractions (Fig. 3B). In contrast, small amount of the D-p53 protein separated in from fraction 6 and 19 (Dc3) or fraction 12 to 16 (Dc4). The N-terminal aa sequences of p64 was LPMLP identical to the 14-18 aa residues of DcHEV ORF2, indicating that D-p64 were derived from the DcHEV ORF2 protein and with ~50 aa deletion at C-terminus. Observation of fractions 9 from both Ac[Dc3n13ORF2] and Ac[Dc4n13ORF2] infected samples by electron microscopy revealed spherical particles with diameters of 35 nm (Fig. 3C, 3D), indicating that the D-p64 protein self-assembled into VLPs. The morphology of these particles similar to native HEV particle and were named as Dc3nVLPs or Dc4nVLPs, respectively.
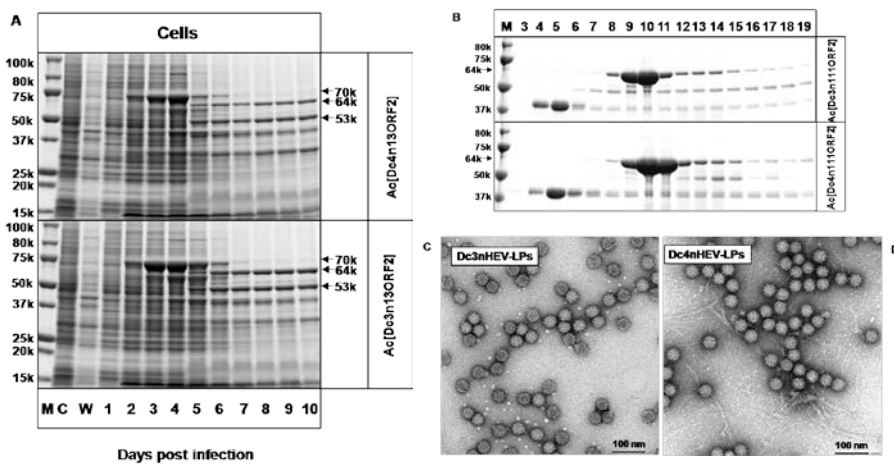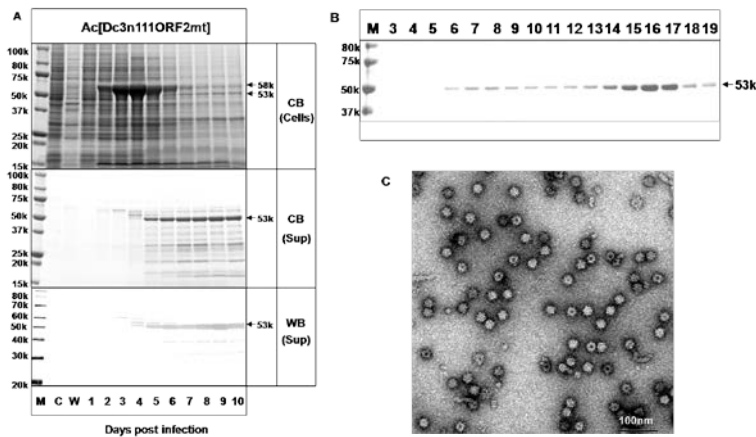

Fig. 3. Expression and purification of VLPs from Ac[Dc3n13ORF2] and Ac[Dc4n13ORF2]-infected Tn5 cells. Time course (A). M, molecular weight marker; C, mock; W, wild-type baculovirus-infected Tn5 cells; lanes 1 to 10, day 1 to 10 p.i.. CsCl fraction were analyzed by electrophoresis and stained with Coomassie blue (B). Native size VLPs were observed by EM (C, D). Bar, 100 nm.

To determine whether nucleic acids were packaged in these VLPs, nucleic acids were extracted from these purified VLPs and analyzed on 1% agarose gel. Electrophoresis results demonstrated that both Dc3nVLPs and Dc4nVLPs contained nucleic acids and that was sensitive for RNase A. By next generation sequence analysis the nucleic sequence identical to N-terminal 13-aa-truncated Dc3 and Dc4 HEV ORF2, indicating that the large particles encapsulated ORF2 genome. In contrast, no nucleic acid was detected from 24 nm VLPs.

The amino acid Met-358 effect T=1 DcsVLPs formation

Comparison of amino acids 111 to 660 between Dc3 and Dc4 ORF2 showed that only two amino acids aa146 and aa358 were different. In Dc3 and Dc4 the aa146 is Thr and Ser, respectively, and both Ser and Thr in aa146 are common among HEVs in the species *Orthohepevirus* A. The aa358 in Dc3 is Met, in Dc4 Thr. Alignment of HEV ORF2 amino acids sequence among 242 HEV strains in the species *Orthohepevirus* A revealed that except rabbit HEV only two strains the aa358 is Met while other aligned sequence is Thr, suggesting that rather than aa146 the Met-358 might be a contributing factor to effect T=1 VLPs formation. To validate this hypothesis, a recombinant baculovirus Ac[Dc3n111ORF2mt] comprising mutated 111-aa-truncated DcHEV ORF2 with the substitution M358T was produced. As shown in Fig. 4, in Ac[Dc3n111ORF2mt]-infected Tn5 cells, a protein migrating with a molecular mass of 53 kDa was found in the cells and supernatant from day 4 p.i.. The amount of the D-p53 protein in the Ac[Dc3n111ORF2mt]-infected Tn5 cell culture supernatant is significant larger than it in Ac[Dc3n111ORF2] and no

small proteins (17-18 kDa) detected. By CsCl gradient centrifugation, proteins, D-p53 mainly appeared in fractions 15-17 fractions with average densities of $1.285g/cm^3$ (Fig. 4B), and VLPs examined by EM possess great similarity with Dcs4VLPs (Fig. 4C). This result indicats that the aa Met-358 affect the T=1 VLPs formation and makes the D-p53 protein unstable.

Fig. 4. Expression and purification of VLPs from mutant M358T of 111-N-terminal aa-truncated Dc3 ORF2 (A). M, molecular weight marker; C, mock-infected Tn5 cells; W, wild-type baculovirus-infected Tn5 cells; lanes 1 to 10, Ac[Dc3n111ORF2mt] -infected Tn5 cells harvested on days 1 to 10 p.i.. CsCl fractions were analyzed by electrophoresis on 5% to 20% polyacrylamide gel, and stained with Coomassie blue (B). The VLPs was observed by EM (C). Bar, 100 nm.
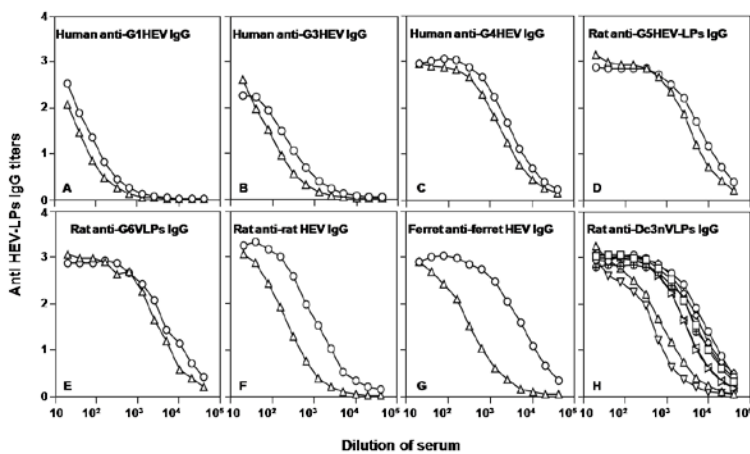

Fig. 5. Antigenic cross-reactivity among ferret, rat, G1, G3-G6 and Dc3nVLPs. Human anti-G1, G3 and G4 HEV IgG, rat anti-G5, G6 and rat HEV-LPs IgG, ferret anti-ferret HEV IgG, was detected by ELISA use Dc3nVLPs as antigen (△) and compared with that detected by each homologues antigen (○) (A-G). Ttiter of rat anti-Dc3nVLPs IgG were determined using ferret VLPs (▽), rat VLPs (△), G1 VLPs (□), G3 VLPs (◇), G4 HEV-LPs (⊕), G5 VLPs (▷), G6 VLPs (◁) and Dc3nVLPs (○) as antigen, respectively (H).

Antigenic cross-reactivity among ferret, rat, G1, G3-G6 and DcHEVs

Western blot analysis indicated that the DcHEV capsid protein D-p53 reacted with rabbit anti-G1 HEV, suggests that the DcHEV has similar antigenicity to G1 HEV. To explore the antigenic cross-reactivity among ferret, rat, G1, G3, G4, G5 and G6 DcHEVs, we detect Human anti-G1, G3 and G4 HEV IgG, rat anti-G5 and G6 HEV-LPs IgG (unpublished data), rat anti-rat HEV-IgG, ferret anti-ferret HEV IgG, by ELISA which use Dc3nVLPs as antigen and compared with that detected by each homologues antigen. As shows in Fig. 5A-E, human anti-G1, G3 and G4 HEV IgG, rat anti-G5 and G6 HEV-LPs IgG, reacted to Dc3nVLPs and each homologous HEV-LPs with similar titers. In contrast, the titer of rat anti-rat HEV-IgG and ferret anti-ferret HEV IgG detected by using of Dc3nVLPs was lower than that detected by homologous HEV-LPs (Fig.5F, G). These results indicated that DcHEV has antigenic epitope(s) common to those of ferret, rat G1, G3 to G6 and DcHEVs, and the antigenicity of DcHEV similar to G1, G3 to G6 HEV than rat and ferret HEV.

To obtain antibody against DcHEV, rat was inoculated with Dc3nVLPs. After three injections, rat elicited a high level of IgG antibodies against Dc3nVLPs, and IgG titers reached as high as 1:819,200 by antibody ELISA. The antibody against Dc3nVLPs reacted not only with Dc3nVLPs, but also with heterologous ferret, rat, G1, G3, G4, G5

and G6 HEV-LPs with titers of 1:51,200, 1:102,400, 1: 819,200, 1:819,200, 1:409,600, 1:409,600, 1:409,600, respectively (Fig. 5H).
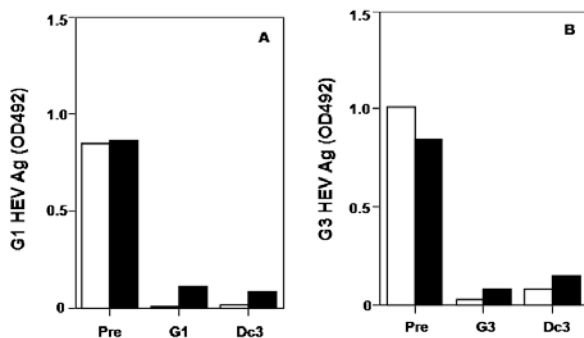
Fig. 6. Neutralizing activity of antibodies against G1 and G3 HEV. Neutralization of G1 and G3 HEV by anti-G1, G3 and Dc3nVLPs sera was carried out by a cell culture based neutralization test. Bars indicate the OD values of HEV Ag. Pre, pre-immunized rat serum; G1, rat anti-G1 HEV-LPs serum; G3, rat anti-G3 HEV-LPs serum; Dc3, rat anti-Dc3nVLPs serum. Rat serum was diluted at 1:10 (white bar), and 1:100 (black bar).

Cross neutralization of G1 and G3 HEV with anti-Dc3nHEV-LPs antibodies

To examine the neutralization activity of anti-Dc3nVLPs antibodies, diluted (1:10 and 1:100) antibodies was mixed with G1 and G3 HEV, respectively, and incubated for neutralization, and then inoculated to PLC/PRF/5 cells. Pre-immunized rat serum was used as the negative control, rat anti-G1 and G3 HEV-LPs antiserum was used as the positive control, respectively. As shown in the Fig. 6, HEV Ag was detected in the samples inoculated with pre-immunized rat serum with the optical density (OD) values ranging from 0.815 to 0.846 (G1), and 0.860 to 1.009 (G3). In contrast, HEV-Ag was not detected in samples incubated with rat serum against G1, G3 and Dc3nVLPs. These results indicated that G1 and G3 HEV were neutralized by antibody against G1, G3 and Dc3nVLPs. In other words, the serotype of DcHEV is identical to G1 and G3 HEVs.

Discussion

Dromedary camel is a new species to harboring HEV, and DcHEV was recently proposed as a new genotype of HEV (G7) in species *Orthohepevirus* A with other HEV strains isolated from human, rabbit or wild boar. Although the DcHEV RNA positive rates was 1.5% in the adult dromedary camel fecal samples, but the sero-prevalence is not clear. Because no cell-culture system has been developed for DcHEV, it remains necessary to express the capsid protein and generate VLPs in order to analyze the antigenicity and immunogenicity of DcHEV, furthermore to establish the method for detection of anti-DcHEV IgG and IgM antibodies.

For produce VLPs, the full-length ORF2 of Dc3 and Dc4 were initially expressed by a recombinant baculovirus; however, the recombinant protein derived from this gene was not released into the culture supernatant and did not form VLPs. However, the native size virus-like particles Dc3nVLPs and Dc4nVLPs were obtained by expressing the N-terminal 13 aa-truncated Dc3 and Dc4 ORF2. As native size VLPs of G3 HEV, nucleic acids were also detected from both Dc3nVLPs and Dc4nVLPs, suggesting that RNA binding might be the extrinsic factor essential for the assembly of HEV native capsid (6).

The Dc4sVLPs was obtained by expressing the N terminal 111-aa deleted Dc4ORF2, that similar to G1, G3, and G4 HEV. An interesting finding is that a naturally occurred substitution from Thr to Met at aa358 of ORF2 causes the abortion of the small VLPs assembly. The naturally occurred single point mutation hampers the T=1 particle assembly by the expressed N-111 truncated proteins.

When rats were immunized with Dc3nVLPs, a strong immune response was induced with high IgG titer in the absence of any adjuvant, suggesting that Dc3nVLPs are highly immunogenic. The antibody induced by the Dc3nVLPs was cross-reactivity with rat, ferret, G1, G3 to G6 HEV-LPs. These results clearly demonstrated that the DcHEV and rat,

ferret, G1, G3 to G6 HEVs share at least one common epitope. The Dc3HEV capsid protein shared higher aa identities (88.5-91.1%) with G1, G3 to G6 HEVs than did rat and ferret HEVs (56.1-56.7 %), and the Dc3nVLPs showed stronger cross-reactivities with anti-G1, G3 to G6 HEV-LPs sera. Furthermore, we found G1 and G3 HEV were neutralized by rat anti-Dc3nVLPs antibody, indicating clearly that the serotype of DcHEV is identical to G1 and G3 HEVs. Because G1-G4 HEVs have been proved to represent a single serotype, we could conclude that the serotype of DcHEV is identical to human HEV.

At present, data other than the nucleotide sequences of the two DcHEV strains from Dubai remain unknown, including the epidemiology, virology and pathology of this virus. The ELISA based on DcnVLPs for detection of anti-DcHEV IgG and IgM will be useful for monitoring the circulation of DcHEV in dromedary camel.

References

1. Balayan MS, Andjaparidze AG, Savinskaya SS, et al. (1983) Evidence for a virus in non-A, non-B hepatitis transmitted via the fecal-oral route. Intervirology 20(1): 23-31.

2. Li TC, Ochiai S, Ishiko H, Wakita T, et al. (2012) A retrospective study on imported hepatitis E in Japan. Travel Med Infect Dis 10(2): 80-85.

3. Tei S, Kitajima N, Takahashi K, et al. (2003) Zoonotic transmission of hepatitis E virus from deer to human beings. Lancet 362(9381): 371-373.

4. Woo PC, Lau SK, Teng JL, et al. (2014) New hepatitis E virus genotype in camels, the Middle East. Emerg Infect Dis 20(6): 1044-1048.

5. Li TC, Yamakawa Y, Suzuki K, et al. (1997) Expression and self-assembly of empty virus-like particles of hepatitis E virus. J Virol 71(10): 7207-7213.

6. Xing L, Li TC, Mayazaki N, et al. (2010) Structure of hepatitis E virion-sized particle reveals an RNA-dependent viral assembly pathway. J Biol Chem 285(43): 33175-33183.

作成日：2015 年 4 月 10 日

Spinal dopaminergic involvement in the antihyperalgesic effect
of antidepressants in rats with neuropathic pain
ラット神経障害性疼痛モデルの抗うつ薬による痛覚過敏抑制作用には
脊髄のドーパミンが関与している

研 究 者 氏 名　　　陳　　覓（第36期笹川医学研究者）

中国所属機関　　　貴陽医学院附属医院麻酔科

日本研究機関　　　群馬大学大学院医学系研究科麻酔神経科学

指 導 責 任 者　　　齋藤　繁　教授，小幡英章　准教授

共同研究者名　　　星野一　博士

Abstract：

　　Mechanical hyperalgesia is one tormenting symptom of neuropathic pain. Thus antidepressants such as tricyclic antidepressants（TCAs）, selective serotonin reuptake inhibitors（SSRIs）and serotonin NA reuptake inhibitors（SNRIs）are first-line treatment for chronic neuropathic pain conditions. However, the efficacy and mechanisms of antihyperalgesic effects of antidepressants have yet to be fully explored. Here, we aimed to reveal the underlying efficacy and mechanisms of antihyperalgesic effects of antidepressants in the animal model of neuropathic pain induced by spinal never ligation（SNL）and whether the effects were reversed by intrathecal injection of sulpride, an antagonist of dopamine D2 receptor. The right L5 spinal nerves of male Sprague Dawley rats were ligated under inhalation anesthesia in order to mimic animal model of peripheral hyperalgesic pain. Behavioral testing was measured after intraperitoneal injection of amitriptyline, fluoxetine, duloxetine and milnacipran. Pretreatment of blocking D2 receptors by intrathecal administration of Sulpride was performed before intraperitoneal treatment of antidepressants. Intraperitoneal injection of amitriptyline (30mg/kg), fluoxetine (10mg/kg and 30mg/kg), duloxetine (30mg/kg) and milnacipran (10mg/kg and 30 mg/kg) produced antihyperalgesic effects from 15 minutes after injection. Pretreatment with sulpride (30μg) reversed the effects (using 30mg/kg antidepressants for each blocking experiment), especially the effect of milnacipran was reversed completely, but the effect of fluoxetine was reversed partially. Our results suggest that antidepressants decreased spinal nerve injury-induced neuropathic pain, which is not only related with NA and 5-HT, but DA also plays a crucial role in spinal cord.

Key Words:

Antidepressants, spinal never ligation, neuropathic pain

1.　Introduction

　　Long-lasting neuropathic pain , as an abnormal pain state caused by an injured peripheral nervous system or central nervous system, is a common event after trauma, chemotherapy or surgery[1,2].

　　Antidepressants, as effective drugs in the treatment of various chronic and neuropathic pain conditions, reveal a large of pharmacological actions as follows: they inhibit the reuptake of noradrenaline(NA) and serotonin（5-HT）, have effects on opioid receptors directly and indirectly, block histamine, cholinergic, 5-hydroxytryptamine and N-methyl-D-aspartate receptors, block ion channel activity, inhibit ectopic afferent discharges and the uptake of adenosine[3,4,5]. The roles of monoaminergic systems, noradrenaline and serotonin in pain pathophysiology have formed the basis, tricyclic antidepressants（TCAs）, selective serotonin reuptake inhibitors（SSRIs）and serotonin NA reuptake inhibitors（SNRIs）are widely used in neuropathic pain treatment[2].

　　Involvement of dopamine (DA) in regulation of pain and particularly in antinociception is being noticed more and more recently. Dopaminergic innervation to the dorsal horn derived from the A11 region in the dorsal posterior hypothalamus [6]. The inhibition of nociceptive transmission at the dorsal horn occurred on the diencephalon spinal

projections of these neurons is mediated by D2 receptors primarily [7]. Therefore, DA in the spinal cord has an analgesic effect result from action on D2 receptors which are located presynaptically and postsynaptically to the spinal dorsal horn neuron [8]. Nevertheless, the role that dopaminergic D2 receptors play in antinociceptive modulation by antidepressants has not been fully understood.

For this purpose, the study was untaken to evaluate the efficacy and mechanisms of antihyperalgesic effects of different antidepressants in the animal model of neuropathic pain elicited by a spinal never ligation. In addition, we determined to investigate whether blocking the D2 receptors by intrathecal administration of Sulpride, a D2 receptors antagonist, prevents the antidepressants-induced antinociception in nerve-injured animals. Besides, we used vivo microdialysis to measure changes of NA, 5-HT and DA contents in lumbar spinal cord after spinal never ligation.

2. Materials and methods

2.1. Experimental animals

The experiments were performed in adult, male Sprague Dawley rats weighing 200-250 g. The right L5 spinal nerves were isolated and tightly ligated with 5–0 silk thread. The wound was sutured after spinal nerve ligation (SNL).A chronic intrathecal catheter was implanted for drug administration 7 days after SNL surgery. The animals were allocated to individual cages to recover for 7 days before drug testing.

2.2. Behavioral testing and drug preparation and delivery

An analgesimeter (Ugo Basile, Comerio, Italy) was used to apply mechanical stimuli in increments (to a maximum of 250 g) to the outer mid-plantar surface of the hind paw until an abrupt foot withdrawal was observed, and the value was recorded [9,10].Animals were administered either amitriptyline(TCAs)(LKT Laboratories Inc. USA), fluoxetine(SSRIs) (Sigma, St. Louis, MO), duloxetine (SNRIs) (Wako Pure Chemical Industries Ltd. Osaka, Japan), milnacipran (SNRIs) (Asahi Kasei Corporation ,Osaka, Japan)or vehicle, at an intraperitoneal injection volume of 500μL. The withdraw threshold was determined at pre-SNL, time 0, time 15, time 30, time 60, then at 60 minutes intervals until 180 minutes after injection. For the blocking experiment, 30μg sulpride (Tocris, Ellisville, MO) was dissolved in mixture of 50% saline and 50% dimethylsulfoxide and treated intrathecally in a volume of 5μL and followed by a 10μL saline to flush the catheter, 15 minutes before all of the antidepressants injection.

2.3. Statistical analysis

Shapiro-Wilk test was applied to verify normal distribution. Homogeneity of variance was analysed by levene's test. Data were normally distributed and equal variance，all the values were expressed as mean ± standard error of means (SEM) for 6 animals per group based on previous study [9]. An independent t test was performed in time point comparisons between 0 min and pre-SNL. Differences among groups were determined using two-way analysis of variance (ANOVA) followed by Bonferroni test was used for *post hoc* analysis. $P < 0.05$ was considered statistically significant. The statistical test was performed by using SPSS 18.0 (SPSS Inc., Chicago).


3. Results

3.1 Antihyperalgesic effect of amitriptyline and related effect of D2 receptor antagonist pretreatment

Intraperitoneal administration of amitriptyline (30mg/kg) attenuated hyperalgesic responses induced by mechanical stimuli (P<0.05; Fig.1 A). Paw withdrawal threshold was increased sharply 15 minutes after intraperitoneal injection and maintained until 180 minutes compared with vehicle group (P<0.05). Significant statistical differences were observed and paw withdrawal threshold was obviously decreased after pretreatment with intrathecal administration of sulpride (30μg) (P<0.05; Fig.1 B). Intrathecal administration of sulpride itself (30μg) did not affect the withdrawal thresholds compared with the vehcile group.

3.2 Antihyperalgesic effect of fluoxetine and related effect of D2 receptor antagonist pretreatment

Intraperitoneal injection of fluoxetine (30mg/kg) produced an antihyperalgesic effect and the effect was observed from 15 minutes after injection. Intraperitoneal treatment of fluoxetine (10mg/kg) also produced an antihyperalgesic effect and the effect was observed from 30 minutes after injection (P<0.05; Fig.2 A). The maximum dose (30mg/kg) was determined to perform in the antagonist experiment. Paw withdrawal threshold was decreased after pretreatment with intrathecal administration of sulpride (30μg) but the statistical difference was observed only in 30 minutes after intraperitoneal injection of fluoxetine (30mg/kg) (P<0.05; Fig.2 B). Intrathecal injection of sulpride itself (30μg) did not affect the withdrawal thresholds.
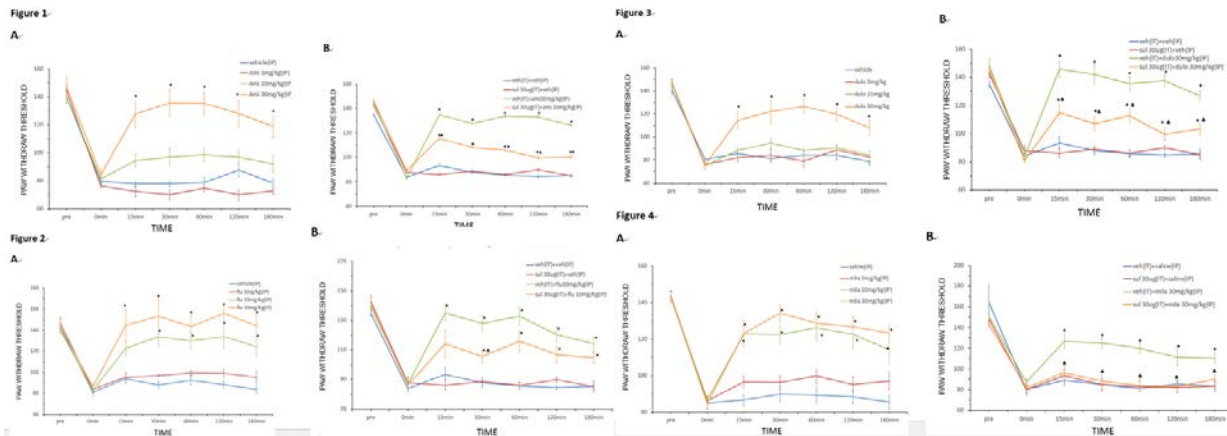
3.3 Antihyperalgesic effects of duloxetine, milnacipran and related effects of D2 receptor antagonist pretreatment

A significant antihyperalgesic effect was observed from 15 minutes after intraperitoneal treatment of duloxetine (30mg/kg) and continued to 180 minutes after injection (P<0.05; Fig.3 A). Intrathecal administration of sulpride (30μg) reversed this effect elicited by duloxetine (30mg/kg) (P<0.05; Fig.3 B). Intraperitoneal injection of milnacipran (10mg/kg and 30 mg/kg) induced antihyperalgesic effects from 15 minutes after injection (P<0.05; Fig.4 A). The maximum dose (30mg/kg) was also determined to perform in the antagonist experiment. Pretreatment with sulpride (30μg) reversed this effect completely (P<0.05; Fig.4 B) and the paw withdrawal threshold was dramatically reduced to nearly the baseline.

4.   Discussion

Indepth exploration of potential mechanisms of antihyperalgesic effects of antidepressants would be a crucial guidance for preventive strategies. The current study provides evidences that intraperitoneal injection of amitriptyline, fluoxetine, duloxetine and milnacipran induced antihyperalgesic effects in SNL rats, and pretreatment with a D2 receptor antagonist reversed the effects. These finding demonstrate that the antidepressants attenuated spinal nerve injury-induced neuropathic pain, and a vital relevance was observed in DA in spinal cord.

4.1 Antihyperalgesic effect of amitriptyline (TCAs)

Mechanical hyperalgesia is a distressing symptom of neuropathic pain which is considered by central sensitization of the nociceptive system [11]. This sensitization can be elicited experimentally with the SNL rats. The tricyclic antidepressants (TCAs) amitriptyline has been extensively investigated in terms of analgesic effects and it has suggested efficacy in clinical trials and in experimental animals [12]. TCAs exert the antinociceptive effects by complicated mechanisms. Block of peripheral nerve sodium channels at therapeutic doses may attenuate acute and chronic pain after surgery [13]. The effect on decrease of activated microglia and astrocytes may contributes to the antihyperalgesic efficacy of TCAs [12]. The antiallodynic effect of TCAs is also mediated by a recruitment of the endogenous opioid system such as delta-opioid receptors, as well as involvement of neuroinflammatory processes modulation, and blocking the reuptake of NA and 5-HT [14]. However, few reports suggest the mechanism which amitriptyline performs its effect on the prevention of mechanical allodynia mediated by DA. In the present study, intraperitoneal injection of amitriptyline induced an antihyperalgesic effect in SNL rats, and the effect was reversed by intrathecal injection of a D2

receptor antagonist. This result suggests the antihyperalgesic effect produced by amitriptyline in SNL rats is related to D2 receptor antagonist.

4.2 Antihyperalgesic effect of fluoxetine (SSRIs)

Fluoxetine, a selective serotonin reuptake inhibitor (SSRIs), is one of the potential agent to treat neuropathic pain which displays distinct selectivity for 5-HT neuronal uptake sites [15]. Although, 5-HT is known to be a crucial neurotransmitter in pain regulation, the mechanism by which fluoxetine exerts its antihyperalgesic effect is still controversial. Previous authors suggest that the concentration of 5-HT was reduced in the raphe magnus nucleus and forebrain of neuropathic animals [16]. Thus, fluoxetine produces its pharmacological effect via the blockade of 5-HT reuptake, increasing 5-HT level in the synaptic cleft and enhancing the efficacy of the 5-HT transmission. Recent reports indicate that upregulation of microglia in the lumbar spinal cord and DRG was observed after sciatic nerve injury-induced pain, which is diminished by fluoxetine treatment. SSRIs generate the antihyperalgesic effect by inhibiting ligand-gated ion channel receptors expressed in microglia. Besides, various 5-HT receptor subtypes, including the 5-HT1A, 5-HT1B, 5-HT2A, 5-HT2C, and 5-HT3 receptors, involved in the modulation of neuropathic pain. In contrast, some researchers suggest that fluoxetine alone fails to suppress nociceptive effects in diabetic and sciatic nerve ligation neuropathy models, but it enhances the analgesic effects of opioid agonists in the periphery. It has been shown that co-administration of morphine with fluoxetine may contribute to the treatment of neuropathic pain[9,15].The current study shows that treatment with fluoxetine induced a significant increase of withdrawal threshold in SNL rats, which is in accordance with other reports. Our data suggests that fluoxetine itself possesses antinociceptive property in spinal nerve injury-induced neuropathic pain. Nevertheless, the antinociceptive effect is reversed by pre-treatment of D2-receptor antagonist only at 30 minutes after intraperitoneal injection of fluoxetine. Although the increase of DA in spinal cord did not produced blocking effect in neuropathic pain strongly, DA still involves in the inhibition of neuropathic pain. The further studies are expected to demonstrate it clearly.

4.3 Antihyperalgesic effects of duloxetine and milnacipran（SNRIs）

As novel antidepressants inhibiting both 5-HT and NA reuptake transporters (SNRIs), duloxetine and milnacipran demonstrate analgesia in clinical trials in patients or experimental animals with peripheral neuropathic pain and fibromyalgia [18]. The antinociceptive effect of inhibitory neurotransmitters is mediated by the activation of descending inhibitory pathways which inhibit pain. Thus the underlying mechanisms include inhibition of 5-HT and NA reuptake leading to enhanced descending inhibition of central sensitization of pain [19]. Similar finding has been reported bulbospinal descending NA and 5-HT systems inhibit nociceptive signals from primary afferent neurons to the spinal dorsal horn neurons via the spinal 5-HT2A and α2-adrenergic receptors [20]. Recent evidences have demonstrated SNRIs elicit antinociceptive or antiallodynic effect with neuropathic pain through α1, α2 adrenoreceptors and 5-HT1A, 5-HT1B receptors [21]]. Furthermore, the inhibition of NA and 5-HT reuptake by antidepressants would enhance amine availability at peripheral nerve terminals [4]. The analgesic efficacy of milnacipran is also observed at the spinal level by inhibiting C-fibre-mediated nociceptive synaptic transmission by activating both the spinal 5-HT and NA systems [22]. Nevertheless, there are several reports suggest that antiallodynic effect of 5-HT depends on the NA level, the more powerful efficacy and release of NA may be necessary for 5-HT to elicit antiallodynic effects [9]. Our data shows duloxetine and milnacipran induced distinct antihyperalgesic effects in SNL rats which is in line with a recent finding that duloxetine delivery produced antihyperalgesic effect in postoperative pain model by increasing spinal 5-HT and NA concentrations[20]. The reversions of mechanical allodynia by pretreatment of D2 receptor antagonist sulpride were observed in both duloxetine and milnacipran, especially the effect of milnacipran was reversed completely. The result reveals that the powerful inhibition of D2 receptor may be responsible for the analgesic effects of duloxetine and milnacipran, and perhaps it was stronger in milnacipran.

Compared with the enormous researches devoted to NA and 5-HT, spinal actions of DA have received deficient

attention. Nevertheless, there are several reports indicate that D2 receptor agonists enhance opioidergic antinociception and the interaction between them is superadditive [6]. Some results support that striatal administration of dopamine D2 receptors attenuated pain-related responses by suppression of impulse discharge of pro-nociceptive neurons in the rostroventromedial medulla, and spinal 5-HT and dopamine D2 receptors were involved in descending pain modulation [8]. Selective activation of the dopamine D2 receptor or blockade of D1 receptor in the rostral agranular insular cortex blunted neuropathic nociception [23]. Previous studies suggest that the activation of mesolimbic dopamine neurons originates from the cell bodies of the ventral tegmental area and projects to the nucleus accumbens, which is an important component in mediating the suppression of pain. Exogenous administration of selective dopamine D2 receptor agonist to nucleus accumbens also exerts an antinociceptive effect [24]. Given the importance of DA system in spinal cord to pain modulation, and interactions with NA and 5-HT systems were focus of attention in our study. It is believed that there is a large-scale plastic changes of nervous system during SNL-induced neuropathic pain in animals [9]. Thus，systemic application of antidepressants suppressed the hyperalgeic effects induced by SNL surgery and the effects reversed by D2 receptor antagonist reveal that antidepressants exit their antihyperalgesic effects via DA levels. In summary, this study has shown beneficial effects of antidepressants on the development of the neuropathic pain after peripheral nerve injury through DA.

References:

1. Jay G W, Barkin R L. Neuropathic pain: etiology, pathophysiology, mechanisms, and evaluations[J]. Disease-a-Month, 2014, 60(1): 6-47.

2. Hache G, Guiard B P, Nguyen T H, et al. Antinociceptive activity of the new triple reuptake inhibitor NS18283 in a mouse model of chemotherapy‐induced neuropathic pain[J]. European Journal of Pain, 2014.

3. Dong X W, Jia Y, Lu S X, et al. The antipsychotic drug, fluphenazine, effectively reverses mechanical allodynia in rat models of neuropathic pain[J]. Psychopharmacology, 2008, 195(4): 559-568.

4. Sawynok J, Esser M J, Reid A R. Antidepressants as analgesics: an overview of central and peripheral mechanisms of action[J]. Journal of Psychiatry and Neuroscience, 2001, 26(1): 21.

5. Lee H G, Choi J I, Yoon M H, et al. The antiallodynic effect of intrathecal tianeptine is exerted by increased serotonin and norepinephrine in the spinal dorsal horn[J]. Neuroscience letters, 2014, 583: 103-107.

6. Millan M J. Descending control of pain[J]. Progress in neurobiology, 2002, 66(6): 355-474.

7. Aira Z, Barrenetxea T, Buesa I, et al. Synaptic upregulation and superadditive interaction of dopamine D2-and μ-opioid receptors after peripheral nerve injury[J]. PAIN®, 2014, 155(12): 2526-2533.

8. Viisanen H, Ansah O B, Pertovaara A. The role of the dopamine D2 receptor in descending control of pain induced by motor cortex stimulation in the neuropathic rat[J]. Brain research bulletin, 2012, 89(3): 133-143.

9. Nakajima K, Obata H, Iriuchijima N, et al. An increase in spinal cord noradrenaline is a major contributor to the antihyperalgesic effect of antidepressants after peripheral nerve injury in the rat[J]. PAIN®, 2012, 153(5): 990-997.

10. Randall L O. A method for measurement of analgesic activity on inflamed tissue[J]. Arch Int Pharmacodyn, 1957, 111: 409-419.

11. Rempe T, Wolff S, Riedel C, et al. Spinal fMRI Reveals Decreased Descending Inhibition during Secondary Mechanical Hyperalgesia[J]. PloS one, 2014, 9(11): e112325.

12. Cheng K I, Wang H C, Chang L L, et al. Pretreatment with intrathecal amitriptyline potentiates anti-hyperalgesic effects of post-injury intra-peritoneal amitriptyline following spinal nerve ligation[J]. BMC neurology, 2012, 12(1).

13. Dick I E, Brochu R M, Purohit Y, et al. Sodium channel blockade may contribute to the analgesic efficacy of antidepressants[J]. The Journal of Pain, 2007, 8(4): 315-324.

14. Burke N N, Finn D P, Roche M. Chronic administration of amitriptyline differentially alters neuropathic pain-related behaviour in the presence and absence of a depressive-like phenotype[J]. Behavioural brain research, 2015, 278: 193-201.

15. Sounvoravong S, Nakashima M N, Wada M, et al. Modification of antiallodynic and antinociceptive effects of

morphine by peripheral and central action of fluoxetine in a neuropathic mice model[J]. Acta biologica Hungarica, 2007, 58(4): 369-379.

16. Goettl V M, Huang Y, Hackshaw K V, et al. Reduced basal release of serotonin from the ventrobasal thalamus of the rat in a model of neuropathic pain[J]. Pain, 2002, 99(1): 359-366.

17. Zychowska M, Rojewska E, Makuch W, et al. The influence of microglia activation on the efficacy of amitriptyline, doxepin, milnacipran, venlafaxine and fluoxetine in a rat model of neuropathic pain[J]. European journal of pharmacology, 2014.

18. Irving G, Tanenberg R J, Raskin J, et al. Comparative safety and tolerability of duloxetine vs. pregabalin vs. duloxetine plus gabapentin in patients with diabetic peripheral neuropathic pain[J]. International journal of clinical practice, 2014, 68(9): 1130-1140.

19. Lim S M, Shin M R, Kang K H, et al. Evaluation of the Neurological Safety of Epidural Milnacipran in Rats[J]. The Korean journal of pain, 2012, 25(4): 228-237.

20. Sun Y H, Li H S, Zhu C, et al. The analgesia effect of duloxetine on post-operative pain via intrathecal or intraperitoneal administration[J]. Neuroscience letters, 2014, 568: 6-11.

21. Kimura M, Saito S, Obata H. Dexmedetomidine decreases hyperalgesia in neuropathic pain by increasing acetylcholine in the spinal cord[J]. Neuroscience letters, 2012, 529(1): 70-74.

22. Ohnami S, Kato A, Ogawa K, et al. Effects of milnacipran, a 5‐HT and noradrenaline reuptake inhibitor, on C‐fibre‐evoked field potentials in spinal long‐term potentiation and neuropathic pain[J]. British journal of pharmacology, 2012, 167(3): 537-547.

23. Coffeen U, López‐Avila A, Ortega‐Legaspi J M, et al. Dopamine receptors in the anterior insular cortex modulate long‐term nociception in the rat[J]. European Journal of Pain, 2008, 12(5): 535-543.

24. Altier N, Stewart J. The role of dopamine in the nucleus accumbens in analgesia[J]. Life sciences, 1999, 65(22): 2269-2287.

作成日：2015年4月9日

日中笹川医学奨学金制度第36期研究者名簿

氏名	中国所属機関	日本研究機関	指導責任者
権　伍勇	厦門長庚医院 眼科	筑波大学医学医療系 眼科学	教授 大鹿　哲郎
陳　　覓	貴陽医学院附属医院 麻酔科	群馬大学大学院医学系研究科 麻酔神経科学	教授 齋藤　　繁
張　文静	山東省血液中心 血液型研究室	東京大学医科学研究所 人癌病因遺伝子分野	教授 村上　善則
劉　志紅	中国医科大学附属第一医院 急診科	東京医科歯科大学難治疾患研究所 難治病態研究部門免疫疾患分野	教授 鍔田　武志
周　顕鳳	南昌市疾病予防控制中心 微生物科	国立感染症研究所 ウイルス第二部	主任研究官 李　　天成
蔡　璐璐	電子科技大学臨床医学院 四川省人民医院 薬学部	京都薬科大学 薬剤学	教授 山本　　昌